COUPLED-CLUSTER SOLUTION OF THE TIME-DEPENDENT SCHRÖDINGER EQUATION FOR ATOMIC NUCLEI

By

David Allen Pigg

Dissertation

Submitted to the Faculty of the

Graduate School of Vanderbilt University

in partial fulfillment of the requirements

for the degree of

DOCTOR OF PHILOSOPHY

in

Physics

August 2012

Nashville, Tennessee

Approved:

David Dean

David Ernst

Thomas Papenbrock

Sait Umar

Kalman Varga

To my wife, Jessica, a miracle dearly-loved

and

To my wonderful family, persistently-supportive

ACKNOWLEDGEMENTS

I am quite indebted for the guidance provided by the members of my Dissertation Committee, Drs. David Dean, David Ernst, Volker Oberacker, Thomas Papenbrock, Sait Umar, and Kalman Varga; for the un-yielding assistance that I have received from Drs. Gaute Hagen, Hai Ah Nam, and Thomas Papenbrock, all members of the nuclear coupled-cluster collaboration at Oak Ridge National Laboratory; and for fruitful discussions with Dr. Simen Kvaal of the University of Oslo. I am especially grateful for the knowledge and honorable advice--both personal and professional--that I have received from Dr. Sait Umar, the Chairman of my Dissertation Committee, throughout my studentship at Vanderbilt University. Without the direction given by--and the vast wealth of knowledge held by--those named here, the work presented in this thesis would remain to be done.

This work has been supported by the U.S. Department of Energy under grant Nos. DE-FG02-96ER40975 (Vanderbilt University), DE-FG02-96ER40963 (University of Tennessee), and DE-AC05-00OR22725 with UT-Battelle, LLC (Oak Ridge National Laboratory). In addition, this work utilized resources of the Oak Ridge Leadership Computing Facility at the Oak Ridge National Laboratory.

Without a doubt, no one has been more supportive of this endeavor than my wife Jessica and my family. I especially thank Jessica for being a light in dark places and for having unwavering patience throughout; and I thank my family for their encouragement and support, both emotional and financial.

PREFACE

This thesis accounts the initial application of time-dependent coupled-cluster theory to solve the quantum many-body problem in nuclear physics. As such, many of the results which are presented here, though unique to the formalism, are not original but have already been obtained within other, more well-known theoretical frameworks.

Throughout, prior knowledge of advanced mathematics, non-relativistic many-body quantum theory, and fundamental nuclear structure is assumed, though in special cases I review such knowledge directly.

TABLE OF CONTENTS

LIST OF TABLES

Table Page

LIST OF FIGURES

CHAPTER I

INTRODUCTION

Atomic nuclei constitute approximately 99.9% of all of the baryonic matter throughout the universe. They are produced within stars; and through fusion reactions therein, they tentatively stabilize star formations. During supernovae explosions, the elements which they compose are scattered across the universe [1]. Nuclei therefore make life possible. Furthermore, nuclei bridge the gap between our understanding of quark-gluon physics—i.e., quantum chromodynamics (QCD)—and macroscopic matter. For these reasons alone, an enduring pursuit of an understanding of the intrinsic and dynamic properties of nuclei is warranted. Of course other, more-practical motivations also exist: after more than a century of work to acquire such understanding, we are now equipped with novel energy resources, defense mechanisms, medicines, imaging techniques, and many other advances that utilize the properties of nuclei and nuclear reactions.

It cannot be challenged that most of this line of success is attributed to the experimental deduction of nuclear properties; in fact, since E. Rutherford's discovery of the nucleus in 1911, a variety of experimental methods have been used to study approximately three thousand nuclei [2]. The known isotopes are shown within the white outline in the Chart of Nuclides, provided in Fig. 1 [3]. The region of the chart which lies beyond the white boundary, commonly called the "Terra incognita" (meaning "unknown land"), contains those nuclides which should in theory exist yet lie beyond the current boundary of experimental exploration. Most of these nuclides—particularly the ones which lie beneath the purple line in the figure, which denotes the astrophysical r-process, the process by which neutrons are rapidly added to a given nucleus, usually during a supernovae—have very small production rates and

extremely small lifetimes which make them impossible to study within a laboratory setting. Because of this limitation and furthermore for the attainment of predicative power, it has been necessary to develop a theoretical framework for studying nuclei.

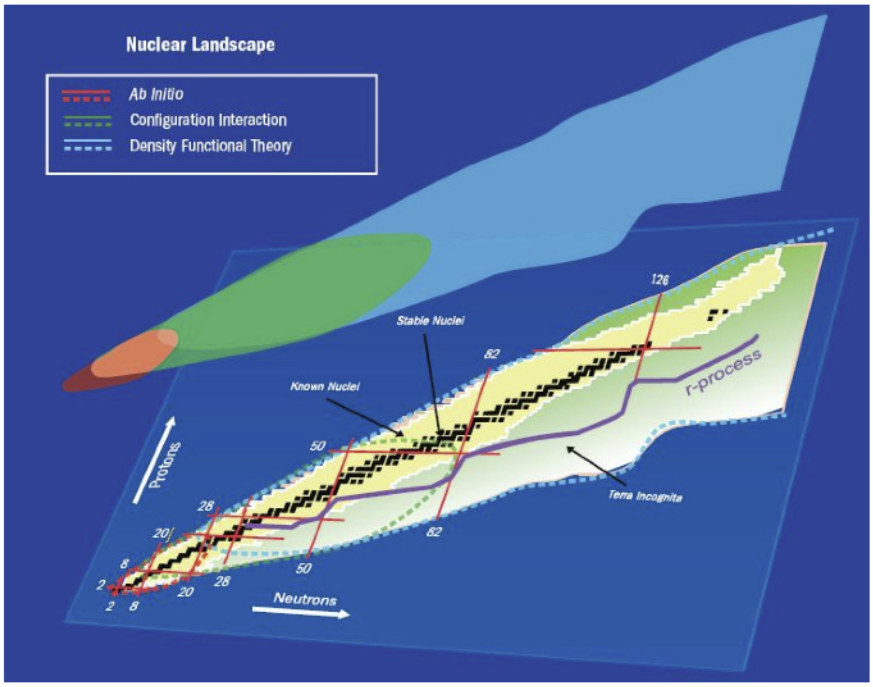

Figure 1. The Chart of Nuclides [3], with neutron (proton) number given along the horizontal (vertical) axis. The region outlined in white contains those nuclides which have been discovered via experiment: specifically, the color black (beige) denotes those nuclides which are (are not) naturally-occurring. The surrounding green region, labeled "Terra incognita," remains unexplored by experiment. The included inset and legend reveals the current reach of each of the three types of nuclear many-body methods: ab initio, configuration interaction, and density functional theory.

Over the past century, many theoretical methods of studying nuclei have been devised. Neglecting the plethora of historical details concerning this development, I simply note that the most significant methods used today may be grouped into the following three categories: density-functional theory, the configuration interaction method [4], and *ab initio* (meaning "from the beginning") methods. While the methods can be said to have advantages and disadvantages relative to each other, it

is clear from the inset of Fig. 1 that they are all in fact complimentary.

In short, density functional theory is based on the assumption that the ground-state observables of a nucleus may be expressed exactly by appropriate functionals of the nucleon density [5]. Though the theory can in principle be related to mean-field methods [6], which rely on the independent particle (or non-interacting shell model) approximation, whereby nucleons are assumed to move about a nucleus within an average potential generated by the other nucleons [7], it is in fact a more-exact method of solving the nuclear many-body problem. However, it does share with mean-field methods a soft computational scaling with system size and thus has been used to study nuclei across the nuclide chart [see the inset of Fig. 1].

The configuration interaction method, which typically utilizes more-realistic approximations of the strong interaction [8], is based on the assumption that the many-body wavefunction has the form

$$|\Psi\rangle = S\,|\Phi\rangle \ , \tag{1}$$

where the operator S is linear in $1p$-$1h$, $2p$-$2h$, ... , Ap-Ah excitation operators and thus generates such excitations within the reference determinant $|\Phi\rangle$. While this method is certainly attractive from a microscopic viewpoint, it has the disadvantage that the computational requirement of its implementation grows exponentially with system size. And while this requirement can be reduced by explicitly truncating the S operator at some np-nh level, where $n < A$, such truncations render computed energies neither size-consistent or size-extensive [4]. Size consistence is the property whereby the total energy of a system of non-interacting fragments is equivalent to the sums of the energies of the individual fragments, and size extensivity is the property whereby the energy scales correctly with system size. From a theoretical viewpoint, adherence to both properties is highly-preferable. For this reason, S is almost never truncated within applications; and in this case, configuration interaction solves the exact nuclear many-body problem. It is notable, however, that if the operator S

is truncated at the $1p$-$1h$ level, the method retains the accuracy of the mean-field Hartree-Fock method [9]. Higher-order truncations of S thus constitute a venue for moving beyond the mean-field approximation. The current reach of the configuration interaction approach, shown in Fig. 1, is restricted relative to that of density functional and mean-field approaches, due to the greater computational requirement associated with incorporating multi-nucleon correlations directly, as is clearly done in Eq. (1).

Ab initio methods, which also employ realistic interactions, are, like the density functional approach, near-exact methods of solving the nuclear many-body problem; however, because they are fully-microscopic, they require much more computational effort than the density functional method—and even the configuration interaction method. This requirement is illustrated by the relatively-small ab initio terrain shown in Fig. 1. While several ab initio methods exist, there are three which pervade the literature: the no-core shell model (NCSM) method [10], the Green's function Monte Carlo (GFMC) method [11], and the coupled-cluster method [12]. In short, the NCSM method involves the direct diagonalization of the nuclear Hamiltonian within a realistic, interacting shell model basis while the GFMC method involves an imaginary-time reduction to the ground-state in which the wavefunction is sampled during the time-propagation. Both of these methods, though quite accurate, have a computational requirement that grows exponentially with system size. For this reason, the coupled-cluster method, which scales only polynomially with system size [13]—though at the cost of some accuracy relative NCSM and GFMC—is often the favorable approach to an ab initio description of the nuclear many-body problem.

Coupled-cluster theory was introduced more than 50 years ago by Coester and Kümmel [14,15] and, because of relatively-soft computational scaling, has since been used to extend ab initio computations into the medium-mass region of the nuclide chart. (Note that recently, even neutron-rich ^{62}Ca has been studied within the

coupled-cluster framework [16]; thus the domain of ab initio computations, as presented in the inset of Fig. 1, is growing, albeit slowly.) In coupled-cluster theory, the many-body wavefunction has the form

$$|\Psi\rangle = e^S |\Phi\rangle \ , \tag{2}$$

where the operator S is the same as in Eq. (1) and $|\Phi\rangle$ is again the reference state. It is by virtue of the exponential in this representation that coupled-cluster theory is both size-consistent and size-extensive—even in the case that S is truncated [4]. Furthermore, the exponential renders a particular truncation in S within the coupled-cluster method more accurate than the identical truncation made within the configuration interaction method: if, for example, $S = S_1 + S_2$, where S_1 (S_2) elicits $1p$-$1h$ ($2p$-$2h$) excitations in the reference state, the expansion of the exponential will contain terms such as S_2^2 and $S_1 S_2$—i.e., higher-order correlations are accounted for as products of lower-order excitation operations. Most importantly, Eq. (2) clearly provides a venue for generating a systematic hierarchy of approximations to the nuclear many-body problem. Considering the substantial growth in both the power and availability of computing resources, this quality is quite an asset. Additionally, as is clarified within Chapter 2, moving to higher-order approximations of coupled-cluster theory is made straightforward through diagrammatic techniques [17].

In the later 1970s, P. Hoodbhoy and J. W. Negele formulated time-dependent coupled-cluster theory in the context of nuclear physics [18], with the aim of eventually applying the method to study nuclear collisions. However, that specific application never materialized; and for several years the usage of the method was relegated to the interaction of Lipkin models [19, 20]. In the early 1980s, the method was adopted for applications within the quantum chemistry community and has since been used only intermittently [21–29]. This sporadic usage is no doubt due to confusion in regard to the definition of energy within time-dependent coupled-cluster theory prior to the bi-variational formulation of the method, first introduced by J. Arponen [30] and very-

recently re-introduced in an explicitly time-dependent framework by S. Kvaal [31]. Throughout this thesis, the source of such confusion will be made clear: outside of the bi-variational formulation of time-dependent coupled-cluster theory, time-evolved energies are not conserved, have no minimum boundary at the ground state, and furthermore can develop imaginary components. It will furthermore be shown that the bi-variational formulation of the method has an energy that is defined by a stationary functional with a complex-analytic time dependence and thus is real and conserved—and furthermore has a minimum boundary at the ground state.

To date, a description of nuclear reactions has been almost exclusive to time-dependent mean-field methods [32–35]. In this thesis, I document the first step toward doing such computations within the ab initio regime. Specifically, I report in detail applications of time-dependent coupled-cluster theory to study the intrinsic properties of nuclei.

This thesis is organized as follows. Chapter 2 entails a discussion of the different approximations made in coupled-cluster theory and a step-by-step re-derivation of the complete bi-variational time-dependent formulation of the method within a time-independent single-particle basis. In addition, every many-body diagram and corresponding equation needed to repeat the applications discussed in Chapter 3 and furthermore formal proofs of the conservation of energy, the conservation of observables that commute with the Hamiltonian, and the reduction to time-independent coupled-cluster theory in the time-independent limit are provided. Chapter 3 entails a discussion of the applications of time-dependent coupled-cluster theory to nuclei thus far. Specifically, a study of the excitation energy of interacting Lipkin systems and a one-body operator for a single Lipkin system is presented and in both cases results are compared with exact results; nuclear excited state energies are computed by taking a Fourier transform of the time-evolved S amplitudes [see Eq. (2)] and are compared with results obtained within the time-independent formalism; energy con-

servation is probed within a study of the real-time evolution of both the bi-variational energy functional and the coupled-cluster Hamiltonian; and the imaginary-time evolution of the coupled-cluster Hamiltonian is shown to be useful in obtaining ground-state properties. Chapter 4 concludes. Throughout, material that is important yet non-essential to the discussion is forwarded to Appendices.

A summary of much of the discussion in Chapters 2 and 3 and most of the results in Chapter 3 is given in Ref. [36], which I have coauthored with G. Hagen, H. Nam, and T. Papenbrock, all members of the nuclear coupled-cluster collaboration at Oak Ridge National Laboratory. It is thus without hesitation noted that a significant part of the work presented here has been a collaborative effort among myself and these fellow physicists. My specific efforts entail a re-derivation of time-dependent coupled-cluster theory [18, 31]; an authorship of high-performance Fortran codes for the numerical implementation of the method; the use of high-performance computing resources at Oak Ridge National Laboratory to run the codes within the applications presented in Chapter 3; the interjection of various ideas and the discovery of various facts related both to the formal development of the theory in Chapter 2 and to the applications in Chapter 3; and the composition of the initial draft of the resulting publication [36].

CHAPTER II

FORMALISM

The framework of time-dependent coupled-cluster theory [18, 31] for the study of dynamic nuclear phenomena is presented, followed by a natural reduction to time-independent coupled-cluster theory [37] for nuclear ground-state properties and the coupled-cluster equations of motion [38] for nuclear excited state properties. First, a brief discussion is given of the common approximations made in coupled-cluster theory and the specific approximation on which this research has been based.

Coupled-Cluster Singles-and-Doubles Approximation

As presented in the Introduction, in coupled-cluster theory, the many-body wavefunction is constructed by acting the exponential of a linear excitation operator on some reference state:

$$|\Psi\rangle \;=\; e^{S}\,|\Phi\rangle \;\;, \tag{3}$$

where e^S is the cluster operator, S is the linear cluster sum, and $|\Phi\rangle$ is an A-fermion (here, *fermion* $\Rightarrow$ *nucleon*) reference state,

$$|\Phi\rangle = \prod_{p=1}^{A} a_p^\dagger\,|0\rangle \;\;, \tag{4}$$

constructed by acting a product of A fermion creation operators $a_p^\dagger$ on the vacuum state $|0\rangle$. Recall that a creation operator $a_p^\dagger$ adds a fermion in the single-particle state (orbital) p; an annihilation operator a_p removes a fermion from orbital p; and a product of an equivalent number n of creation and annihilation operators $a_{p_1}^\dagger \ldots a_{p_n}^\dagger a_{q_1} \ldots a_{q_n}$ moves n fermions from orbitals $q_1 \ldots q_n$ to orbitals $p_1 \ldots p_n$. Second-quantized operator products of this type appear throughout coupled-cluster

theory. For example, the cluster sum S in Eq. (3) is itself a sum of operators $S_1, S_2, S_3, \ldots, S_A$ which generate 1-particle-1-hole ($1p$-$1h$), $2p$-$2h$, $3p$-$3h$, and up to Ap-Ah excitations, respectively, from the reference state $|\Phi\rangle$:

$$S = S_1 + S_2 + S_3 + \ldots + S_A \ , \tag{5}$$

where the specific form of the np-nh operator S_n is given by

$$S_n = \frac{1}{(n!)^2} \sum_{i_1 \ldots i_n, a_1 \ldots a_n} s_{i_1 \ldots i_n}^{a_1 \ldots a_n} a_{a_1}^\dagger \ldots a_{a_n}^\dagger a_{i_n} \ldots a_{i_1} \ . \tag{6}$$

Throughout this thesis, the indices i, j, k, ... will be used to label orbitals which are occupied in the reference state $|\Phi\rangle$ (hole states); the indices a, b, c, ... will be used to label orbitals which are unoccupied in $|\Phi\rangle$ (particle states); and the indices p, q, r, ... will be used to label any orbital, whether occupied or unoccupied in $|\Phi\rangle$. With this practice in mind, it becomes clear that the operator product in Eq. (6), $a_{a_1}^\dagger \ldots a_{a_n}^\dagger a_{i_n} \ldots a_{i_1}$, is an n-fermion excitation operator: it serves to "excite" n fermions from the occupied orbitals $i_1 \ldots i_n$ to the unoccupied orbitals $a_1 \ldots a_n$. Each excitation has an associated amplitude $s_{i_1 \ldots i_n}^{a_1 \ldots a_n}$, and the pre-factor $1/(n!)^2$ is included to correct for over-counting, since the summation is unrestricted relative to both the occupied and unoccupied sub-spaces.

Taking Eqs. (3), (5), and (6) into consideration, the expansion of the cluster operator e^S in Eq. (3), given by

$$\begin{aligned} e^S &= 1 + S + \frac{1}{2}S^2 + \frac{1}{3!}S^3 + \ldots \\ &= 1 + S_1 + S_2 + \ldots + \frac{1}{2}S_1^2 + \frac{1}{2}S_2^2 + \ldots + S_1 S_2 + \ldots \\ &\quad + \frac{1}{3!}S_1^3 + \frac{1}{3!}S_2^3 + \ldots + \frac{1}{2}S_1 S_2^2 + \frac{1}{2}S_1^2 S_2 + \ldots \ , \end{aligned} \tag{7}$$

clearly generates every possible single-fermion and multi-fermion excitation from the reference state $|\Phi\rangle$, yielding an exact representation for the many-body wavefunction $|\Psi\rangle$. In fact, one can easily derive that such a representation is equiva-

lent to the infinite-order expansion of the many-body perturbation theory wavefunction [4]. While this exactness is attractive from a theoretical viewpoint, in practical applications, it leads to an implementation of coupled-cluster theory that is far too computationally-cumbersome for all but the lightest systems. As I will discuss in detail throughout the next section, any implementation of coupled-cluster theory involves the computation of elements of an e^S-similarity-transformed Hamiltonian $\overline{H} \equiv e^{-S} H e^S$, taken between the reference state and states formed by exciting the reference—i.e., elements such as $\langle \Phi_{i_1}^{a_1} | \, \overline{H} \, | \Phi \rangle$, $\langle \Phi_{i_1 i_2}^{a_1 a_2} | \, \overline{H} \, | \Phi \rangle$, $\ldots$, $\langle \Phi_{i_1 i_2 \ldots i_n}^{a_1 a_2 \ldots a_n} | \, \overline{H} \, | \Phi \rangle$. If $n = A$, the scaling for a *one-time* computation of these elements is $O^A U^{A+2}$, where O is the number of occupied orbitals and U is the number of unoccupied orbitals accounted for within the selected model space [13]. Furthermore, since a typical implementation of the method requires the iterative computation of these elements, such a computation would be tantamount to a full diagonalization of the A-body Hamiltonian and is thus impractical. It is therefore common to truncate the cluster sum S at some level S_e, $e < A$, and thus reduce the number of elements of $\overline{H}$ that must be iteratively computed to e and the scaling to $O^e U^{e+2}$.

The most trivial truncation of S, whereby $S = S_1$, is known as the coupled-cluster with singles approximation (CCS). I describe this approximation as most-trivial since, by the Brillouin Theorem, elements of a Hamiltonian between a Hartree-Fock (HF) wavefunction and a singly-excited wavefunction are identically zero: $\langle \Phi_i^a | \, H \, | \Phi_{HF} \rangle = 0$ [39]. Thus the element $\langle \Phi_i^a | \, \overline{H} \, | \Phi_{HF} \rangle$, which must be iteratively computed during the implementation, is identically zero; and, as I will later clarify, this implies that $s_i^a = 0$ and thus $S = S_1 = 0$, leaving zero contribution to the coupled-cluster correlation energy. In light of this fact, the most-strict-yet-non-trivial approximation is the coupled-cluster with doubles approximation (CCD), whereby $S = S_2$, the implementation of which requires the iterative computation of the element $\langle \Phi_{ij}^{ab} | \, \overline{H} \, | \Phi \rangle$. A more accurate approximation which requires only slightly more computational effort

than CCD is the coupled-cluster with singles-and-doubles (CCSD) approximation, whereby $S = S_1 + S_2$, the implementation of which requires the iterative computation of both elements $\langle \Phi_i^a | \overline{H} | \Phi \rangle$ and $\langle \Phi_{ij}^{ab} | \overline{H} | \Phi \rangle$. The CCSD approximation is arguably the most common approximation made in coupled-cluster theory to date. In terms of accuracy, it has been found to account for roughly 90% of the ground-state correlation energy of the ^{40}Ca nucleus, while the next common higher-order approximation, known as CCSD with triples corrections (CCSD-T), whereby $S = S_1 + S_2 + \delta S_3$, where δS_3 represents the most significant S_3 contributions, accounts for almost all of the remaining 10% of the correlation energy [40, 41]. Higher-order approximations, such as full CCSDT ($S_{max} = S_3$), CCSDTQ ($S_{max} = S_4$), etcetera, are much more computationally-intensive and contribute very little to the ground-state correlation energy; yet in special cases—involving high-energy phenomena, phase transitions, etcetera—such approximations are often necessary to maintain an acceptable level of accuracy [42].

Since the research presented here has involved proof-of-principle applications of time-dependent coupled-cluster theory to study some intrinsic properties of low-energy nuclei, the CCSD approximation has been used within almost all of the computations. In this way, an acceptable balance between accuracy and computational requirement—iteratively, O^2U^4—has been achieved.

Time-Dependent Coupled-Cluster Theory

It is well-known that the implementation of a time-dependent many-body theory for a non-relativistic system involves the solution of the time-dependent Schrödinger equation,

$$H(t) \, |\Psi(t)\rangle \;\; = \;\; i\hbar\partial_t \, |\Psi(t)\rangle \;\; , \tag{8}$$

where H is, in general, a time-dependent Hamiltonian; and, in the coupled-cluster

case, the many-body wavefunction $|\Psi\rangle$ takes the form

$$|\Psi(t)\rangle \;=\; e^{S(t)}\,|\Phi(t)\rangle \;\;. \tag{9}$$

Here the time-dependence of the cluster sum S and the reference state $|\Phi\rangle$ result from the time-dependence of the excitation amplitudes $s^{a_1\ldots a_n}_{i_1\ldots i_n}$ and the second quantized operators $a^\dagger_p$ and a_p [see Eqs. (6) and (4)]. Explicitly, in the CCSD approximation,

$$\begin{aligned} S &= S_0(t) + S_1(t) + S_2(t) \\ &= s_0(t) + \sum_{ia} s^a_i(t) a^\dagger_a(t) a_i(t) + \frac{1}{4}\sum_{ijab} s^{ab}_{ij}(t) a^\dagger_a(t) a^\dagger_b(t) a_j(t) a_i(t) \;, \end{aligned} \tag{10}$$

where the $0p$-$0h$ amplitude s_0 is a complex phase added for completeness; and

$$|\Phi(t)\rangle = \prod_{p=1}^{A} a^\dagger_p(t)\,|0\rangle \;\;, \tag{11}$$

where the time-dependence of the second quantized operators is given as [18]

$$\dot{a}^\dagger_p(t) = \sum_q \langle q(t)|\dot{p}(t)\rangle a^\dagger_q(t) \;, \tag{12}$$

shown here only for the creation operator $a^\dagger_p$. As is done in Eq. (12), I will often use a dot to signify a time derivative. Furthermore, to simplify notation, I will henceforth suppress the time arguments of both the amplitudes and the second quantized operators.

From Eqs. (8)–(11), it is clear that the objective of a time-dependent CCSD (TD-CCSD) implementation is to time-evolve the amplitudes s_0, s^a_i, and s^{ab}_{ij} and the second quantized operators $a^\dagger_p$ and a_p—i.e., the single-particle orbitals—and to thereby obtain the time-evolved many-body wavefunction $|\Psi\rangle$. However, it is perhaps unclear at this point that such an approach is incomplete. To see why, consider the expectation value of the total energy, defined as

$$E \;\equiv\; \langle\tilde{\Psi}|\,H\,|\Psi\rangle \;\;, \tag{13}$$

where $\langle\tilde{\Psi}|$ and $|\Psi\rangle$ are the bra (left) and ket (right) many-body wavefunctions. Prior to expanding this expression, I exercise a bit of foresight by clarifying that in order to derive for the amplitudes working equations which are decoupled from the total energy, it is common practice and in fact essential [14, 43] to expand the left many-body wavefunction in part as $\langle\tilde{\Psi}| = \langle\tilde{\Phi}|\, e^{-S}$. That is, the cluster operator $e^{S} \rightarrow e^{-S}$ on the left-hand side, *not* $e^{S^{\dagger}}$. With this and Eq. (9) in mind, it is clear from the partial expansion of the total energy,

$$E = \langle\tilde{\Phi}|\, e^{-S} H e^{S}\, |\Phi\rangle \tag{14}$$

$$\equiv \langle\tilde{\Phi}|\, \overline{H}\, |\Phi\rangle \ , \tag{15}$$

that the "effective" Hamiltonian $\overline{H} \equiv e^{-S} H e^{S}$ of coupled-cluster theory, given by the e^{S}-mediated similarity-transformation of the Hermitian Hamiltonian H, is non-Hermitian by construction. Accordingly, the states $\langle\tilde{\Phi}|$ and $|\Phi\rangle$ are not adjointly-related; therefore, to attain an admissible TD-CC implementation, one must time-evolve *both* the left and right wavefunctions $\langle\tilde{\Psi}|$ and $|\Psi\rangle$. Essentially, as shown recently by S. Kvaal [31], TD-CC must be formulated as a bi-variational method.

Though $|\Psi\rangle$ is given by Eq. (9)—i.e., it is parameterized by the excitation amplitudes $s^{a_1 \ldots a_n}_{i_1 \ldots i_n}$ and their products according to the expansion of the operator e^{S}—the appropriate parameterization of $\langle\tilde{\Psi}|$ is not immediately apparent. However, in the context of coupled-cluster response methods [21, 26, 30], chemists have shown that the parameterization given by

$$\langle\tilde{\Psi}| \equiv \langle\Phi|\, \Lambda e^{-S} \ , \tag{16}$$

where Λ is a linear de-excitation operator of the form

$$\Lambda = 1 + \sum_{ia} \lambda^{i}_{a} a^{\dagger}_{i} a_{a} + \frac{1}{4} \sum_{ijab} \lambda^{ij}_{ab} a^{\dagger}_{i} a^{\dagger}_{j} a_{b} a_{a} \tag{17}$$

in the CCSD approximation, leads to a stationary functional for the total energy,

given by

$$\mathbb{E} \;=\; \langle\Phi|\,\Lambda\overline{H}\,|\Phi\rangle \;. \tag{18}$$

In Eq. (17), λ_a^i and λ_{ab}^{ij} are probability amplitudes associated with $1h$-$1p$ and $2h$-$2p$ de-excitations, respectively. An excellent account of the details of the parameterization in Eq. (16) and the resulting functional in Eq. (18) is given by I. Shavitt and R. J. Bartlett in Ref. [4]: in short, if we consider the derivative of the similarity-transformed Hamiltonian $\overline{H}$ with respect to some parameter λ, we obtain

$$\overline{H}^{\lambda} \;=\; e^{-S}H^{\lambda}e^{S} + \left[\overline{H}, S^{\lambda}\right] \;, \tag{19}$$

where the superscripts are indicative of the derivatives. Since the commutator in this expression can be written as $\Lambda_{12}(\lambda)e^{-S}H^{\lambda}e^{S}$, where $\Lambda_{12}(\lambda)$ is linear in $1p$-$1h$ and $2p$-$2h$ de-exciations, such that

$$\overline{H}^{\lambda} \;=\; \Big(1 + \Lambda_{12}(\lambda)\Big)e^{-S}H^{\lambda}e^{S} \;, \tag{20}$$

the corresponding energy derivative is given by

$$E^{\lambda}P \;=\; P\Big(1 + \Lambda_{12}(\lambda)\Big)e^{-S}H^{\lambda}e^{S}P \;, \tag{21}$$

where P is an operator which acts to project onto the space of occupied orbitals. The λ integral of Eq. (21) is then given by the functional $\mathbb{E}$ in Eq. (18); and it follows that the left many-body wavefunction must have the form in Eq. (16)—i.e., $\langle\tilde{\Phi}| = \langle\Phi|\,\Lambda$, where $\langle\Phi| = |\Phi\rangle^{\dagger}$. Throughout, it will become clear that this parameterization of the left wavefunction leads to closed-form expressions for observables, the conservation of energy, and the conservation of any observable which commutes with the Hamiltonian; thus it is attractive from a theoretical viewpoint.

With the parameterization in Eq. (16) in mind, it is now clear that, in a TD-CCSD implementation, one must time-evolve the de-excitation amplitudes λ_a^i and

λ_{ab}^{ij} in addition to the excitation amplitudes s_0, s_i^a, and s_{ij}^{ab} and the second quantized operators $a_p^\dagger$ and a_p.

To simplify the implementation within the applications presented in Chapter 3, I neglect the time dependence of the orbitals. In this case, $\dot{a}_p^\dagger = 0 = \dot{a}_p$—i.e., the reference state $|\Phi\rangle$ is time-independent; and the only unknowns are the excitation and de-excitation amplitudes. Furthermore, I use a time-independent, two-body Hamiltonian of normal-ordered form:

$$H_N \;=\; \sum_{pq} f_q^p \{a_p^\dagger a_q\} + \frac{1}{4}\sum_{pqrs} g_{rs}^{pq} \{a_p^\dagger a_q^\dagger a_s a_r\} \;. \tag{22}$$

Here the curly brackets $\{\ldots\}$ are indicative that the second-quantized operators are normal-ordered relative to the Fermi vacuum; the pre-factor $1/4$ is included to correct for over-counting since the summation is unrestricted relative to both the indices of the annihilation operators and those of the creation operators; and f_q^p and g_{rs}^{pq} are elements of the normal-ordered one-body and two-body interactions, which are referred to throughout as F_N and G_N, respectively. Though these elements are typically written as $\langle p||q\rangle$ and $\langle pq||rs\rangle$, respectively, I write them in the forms shown here with foresight that doing so will render the algebraic expressions involving these elements much less cumbersome and more easily understood. Note that the full two-body Hamiltonian H comprises both its Fermi vacuum expectation value,

$$\langle\Phi|\, H \,|\Phi\rangle = \sum_i \langle i||i\rangle + \frac{1}{2}\sum_{ij}\langle ij||ij\rangle \;, \tag{23}$$

and H_N, such that $H = \langle\Phi|\, H \,|\Phi\rangle + H_N$; however, since we are primarily interested in how the correlations induced by the cluster operator e^S influence properties, we should consider only H_N throughout the re-derivation of the theory. For this reason, I define $\overline{H}_S \equiv e^{-S} H_N e^S$.

The S amplitude equations

To re-derive equations for the time-evolution of the excitation amplitudes s_o, s_i^a, and s_{ij}^{ab}, we first use the ansatz in Eq. (9) and left-multiply the time-dependent

Schrödinger equation [see Eq. (8)] by the operator e^{-S}, such that

$$\overline{H}_S|\Phi\rangle \;=\; i\hbar e^{-S}\partial_t e^S|\Phi\rangle \;, \tag{24}$$

written in terms of the the normal-ordered Hamiltonian H_N. To compute the e^S-mediated similarity-transformations of operators H_N and ∂_t, we can employ the Baker-Campbell-Hausdorff expansion [44–46],

$$\begin{aligned} e^{-S}Oe^S \;=\;& O + [O,S] + \frac{1}{2!}[[O,S],S] \\ &+ \frac{1}{3!}[[[O,S],S],S] \\ &+ \frac{1}{4!}[[[[O,S],S],S],S] + \dots \;, \end{aligned} \tag{25}$$

shown here for some operator O.

Before using Eq. (25) to expand $\overline{H}_S$ straightaway, it is instructive to look at the simplest such commutation involved, that between F_N and S_1. Ignoring the indice summations and the coefficients f_q^p and s_i^a, we have

$$\begin{aligned} [a_p^\dagger a_q, a_a^\dagger a_i] \;=\;& a_p^\dagger a_q a_a^\dagger a_i - a_a^\dagger a_i a_p^\dagger a_q \\ =\;& \{a_p^\dagger a_q a_a^\dagger a_i\} + \{a_p^\dagger a_q a_a^\dagger a_i\}_C - \{a_a^\dagger a_i a_p^\dagger a_q\} - \{a_a^\dagger a_i a_p^\dagger a_q\}_C \\ =\;& \{a_p^\dagger a_q a_a^\dagger a_i\}_C - \{a_a^\dagger a_i a_p^\dagger a_q\}_C \\ =\;& \{a_p^\dagger a_q a_a^\dagger a_i\}_C \\ =\;& \{a_p^\dagger \overbrace{a_q a_a^\dagger} a_i\} + \{\overbrace{a_p^\dagger a_q a_a^\dagger} a_i\} + \{\overbrace{a_p^\dagger \overbrace{a_q a_a^\dagger} a_i}\} \\ =\;& \{a_p^\dagger a_i \delta_{qa}\} + \{a_q a_a^\dagger \delta_{pi}\} + \delta_{qa}\delta_{pi} \;. \end{aligned} \tag{26}$$

For the second equality, I have used the generalized Wick's theorem [47], where $\{\dots\}_C$ represents the sum over all normal-ordered products in which there are non-zero single, double, etcetera contractions between the second-quantized operators of F_N and S. For the third equality, I have used the anti-commutative property of mixed products of second-quantized operators and the fact that each operator product contains an even number of creation and annihilation operators; thus $\{F_N S\} = \{S F_N\}$. The

remaining equalities result from the fact that the only surviving contractions are of the forms $\overbrace{a_a a_b^\dagger} = \delta_{ab}$ and $\overbrace{a_i^\dagger a_j} = \delta_{ij}$. From these details, one can deduce that the expansion of $\overline{H}_S$ is simplified in two ways. First, from the sixth equality in Eq. (26), it is clear that each commutation operation in Eq. (25) reduces the number of general-indexed (p, q, r, ...), second-quantized operators by at least one; therefore, since a two-body H_N contains at most four such operators, the expansion of $\overline{H}_S$ truncates naturally at the fourth nested commutator of Eq. (25). Second, the fourth equality clarifies that the only surviving terms in the expansion of $\overline{H}_S$ are those for which H_N has at least one non-zero contraction with every S_n operator on its right—i.e., $\{a_{a_1}^\dagger \dots a_{a_n}^\dagger a_{i_1} \dots a_{i_n} a_{p_1}^\dagger \dots a_{p_n}^\dagger a_{q_1} \dots a_{q_n}\}_C = 0$. Therefore, for $O = H_N$, the expansion in Eq. (25) reduces to

$$\overline{H}_S \;=\; H_N + \overbrace{H_N S} + \frac{1}{2}\overbrace{H_N S S} + \frac{1}{3!}\overbrace{H_N S S S} + \frac{1}{4!}\overbrace{H_N S S S S} \;, \tag{27}$$

where the multi-commutations represent sums over the surviving terms. In the context of many-body diagrams [4], of which I will provide an overview later in this section, Eq. (27) is indicative that the expansion of the coupled-cluster Hamiltonian $\overline{H}_S$ comprises all possible diagrams in which H_N is connected to up to four S_n operators. Note that the restriction to four S_n operators is *only* the result of using a two-body Hamiltonian. In applications using three-body Hamiltonians, for example, the expansion of $\overline{H}_S$ continues through the sixth nested commutator in Eq. (25).

For $O = \partial_t$, the expansion in Eq. (25) reduces to

$$e^{-S}\partial_t e^S \;=\; \partial_t + \dot{S} + \frac{1}{2}[\dot{S}, S] \;, \tag{28}$$

since $[\partial_t, S] \to \dot{S}$ in the approximation that $|\Phi(t)\rangle = |\Phi(0)\rangle$ and the expansion of $[\dot{S}, S]$ yields only terms involving excitation operator products of the form $a_a^\dagger a_i$; hence $[[\dot{S}, S]S] = 0$, along with all higher nested commutators.

With the expansions of $\overline{H}_S$ and $e^{-S}\partial_t e^S$ [see Eqs. (27) and (28)] known, we left project Eq. (24) with the $0p$-$0h$, $1p$-$1h$, and $2p$-$2h$ excited determinants $\langle\Phi|$, $\langle\Phi_i^a|$, and

$\langle \Phi_{ij}^{ab}|$ and thereby obtain

$$i\hbar \dot{s}_0 = \langle \Phi | \, \overline{H}_S \, | \Phi \rangle \tag{29}$$

$$i\hbar \dot{s}_i^a = \langle \Phi_i^a | \, \overline{H}_S \, | \Phi \rangle \tag{30}$$

$$i\hbar \dot{s}_{ij}^{ab} = \left\langle \Phi_{ij}^{ab} \right| \overline{H}_S \, | \Phi \rangle \tag{31}$$

for the time-evolution of the amplitudes s_0, s_i^a, and s_{ij}^{ab}. To the left-hand sides of these equations, only the $\dot{S}$ term of Eq. (28) contributes since the elements of both ∂_t and $\frac{1}{2}[\dot{S}, S]$ are written in terms of only integrals of the type $\langle \dot{p}|q\rangle$ and thus contribute nothing for a time-independent basis. For the interested reader, in Appendix A, I provide the left-hand sides of Eqs. (29)-(31) within a time-dependent basis. To obtain algebraic expressions for the right-hand sides—i.e., for the pertinent matrix elements of $\overline{H}_S$—I use the diagrammatic techniques made well-known by S. A. Kucharski and R. J. Bartlett [17].

In brief, a coupled-cluster diagram is a pictorial representation of some type of correlation between the ket (right) state and the bra (left) state, located below and above the diagram, respectively. Fig. 2, for example, represents a particular connection between the two-body interaction element g_{ab}^{ij}, shown as a dotted line with two de-excitation vertices, denoted in operator form as $a_i^\dagger a_a$ and $a_j^\dagger a_b$, and the $2p$-$2h$ excitation amplitude s_{ij}^{ab}, shown as a continuous line with the two vertices $a_a^\dagger a_i$ and $a_b^\dagger a_j$. Note that lines representing hole states $i, j, k, \ldots$ and particle states $a, b, c, \ldots$ are always directed downward and upward, respectively.

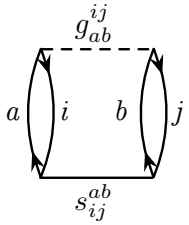

Figure 2. Coupled-cluster diagram example.

The correlation represented by the diagram in Fig. 2 is deemed *closed* since every line in the diagram terminates on a vertex at both top and bottom (and is thus called an *internal* line); thus it is clear that the diagram can only contribute to the element $\langle\Phi|\,\overline{H}_S\,|\Phi\rangle \equiv \overline{H}_0$, which appears on the right-hand side of Eq. (29). Specifically, the diagram represents the contraction $\langle\Phi|\,\overbrace{G_N S_2}\,|\Phi\rangle$, accounted for in the second term of Eq. (27) and given in operator form by

$$\langle\Phi|\,\overbrace{G_N S_2}\,|\Phi\rangle \;=\; \frac{1}{16}\sum_{pqrs}\sum_{ijab} g_{rs}^{pq} s_{ij}^{ab}\,\langle\Phi|\,\{a_p^\dagger a_q^\dagger a_s a_r\}\{a_a^\dagger a_b^\dagger a_j a_i\}\,|\Phi\rangle \;. \tag{32}$$

Though this expression can be simplified with a straightforward application of Wick's theorem, it would be quite tedious to rely on such an application to simplify more than just a few of the contractions within the expansion of $\overline{H}_S$. As I will exemplify, the idea behind the diagrammatic approach is to first pictorially generate all of the contributions to a given element of some operator and to then interpret the pictures algebraically.

Finding the remaining diagrams that contribute to $\overline{H}_0$ is simply a matter of finding the other closed diagrams allotted for in Eq. (27)—i.e., finding all of the closed diagrams which can be formed by connecting one element of H_N with up to four S amplitudes. Taking into account the possible structures of the interaction (F_N and G_N) and amplitude (S_1 and S_2) diagram fragments, which I provide in Appendix B, it is clear that the only such possibilities are those shown in Fig. 3, where for convenience I have suppressed explicit labeling of the interaction and excitation vertices as well as that of the particle and hole lines. Note in the figure that one-body interaction elements f_q^p and $1p$-$1h$ excitation amplitudes s_i^a are represented by dotted and continuous lines, respectively, having only one vertex.

Now that we have a pictorial representation of $\overline{H}_0$, we can obtain the associated algebraic expressions by following the rules for interpreting diagrams, which I provide

in Appendix C. The result is given by

$$\overline{H}_0 \;=\; \sum_{ia} f_a^i s_i^a + \frac{1}{2}\sum_{ijab} g_{ab}^{ij} s_i^a s_j^b + \frac{1}{4}\sum_{ijab} g_{ab}^{ij} s_{ij}^{ab} \;, \tag{33}$$

where the terms appear in the same order as the diagrams in Fig. 3. Note that all of the indices "cancel" from top to bottom, this being indicative that every term is represented by a closed diagram and thus contributes to $\overline{H}_0$. Since some expressions can be quite tedious, such cancellation is a nice check for errors.

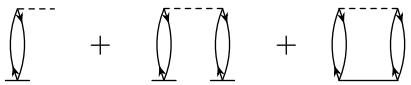

Figure 3. Diagrammatic expansion of the element $\overline{H}_0$.

Finding all of the diagrams in Fig. 3 was clearly a matter of guesswork; however, finding those which contribute to the element $\langle \Phi_i^a | \, \overline{H}_S \, | \Phi \rangle \equiv \overline{H}_i^a$, which appears on the right-hand side of Eq. (30), is somewhat more involved since there are many such possibilities. Specifically, we need to find all of the diagrams associated with the fully-contracted terms of $\langle \Phi | \, \{a_i^\dagger a_a\} \overline{H}_S \, | \Phi \rangle$—that is, we must find all of the topologically-unique diagrams allotted for in Eq. (27) which have one pair of lines ($a_a^\dagger$,a_i) that do not terminate on a vertex (*external* lines). Though even in this case clever guesswork will suffice to generate most—if not all—of the possibilities, it can sometimes be difficult to determine whether or not a given possibility is unique without depending on its algebraic interpretation. Fortunately, a proven method exists for generating all of the unique diagrammatic contributions to any particular element [17]. Without going into exemplary detail, the method is to distinguish the particle and hole lines of each contributing fragment by labeling them with + and −, respectively; then finding all of the unique ways in which the fragments can be connected in such a way as to replicate the character of the element desired is reduced to simply finding all of the

unique sign combinations that will produce that character. For specific examples, see Refs. [4, 37, 48]. Without further explanation, all of the unique contributions to the element $\overline{H}_i^a$ are shown in Fig. 4. Note the diagrammatic representation of $\overline{H}_i^a$ on the left-hand side of the figure. Aside to the element $\overline{H}_0$, it is almost essential to represent the elements of $\overline{H}_S$ diagrammatically since they contribute to many quantities throughout.

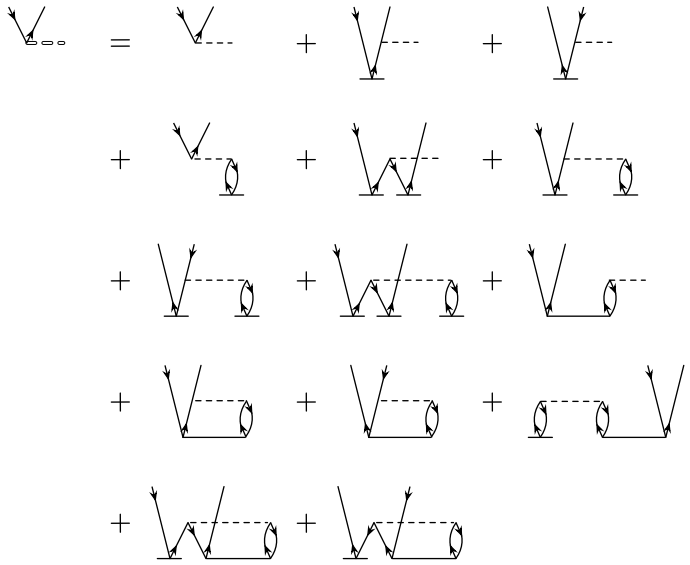

Figure 4. Diagrammatic expansion of the element $\overline{H}_i^a$.

The algebraic expressions associated with the diagrams in Fig. 4 are given by

$$\begin{aligned}
\overline{H}_i^a &= f_i^a + \sum_b f_b^a s_i^b - \sum_j f_i^j s_j^a + \sum_{jb} g_{ib}^{aj} s_j^b - \sum_{jb} f_b^j s_i^b s_j^a \\
&+ \sum_{jbc} g_{bc}^{aj} s_i^b s_j^c - \sum_{jkb} g_{ib}^{jk} s_j^a s_k^b - \sum_{jkbc} g_{bc}^{jk} s_i^b s_j^a s_k^c + \sum_{jb} f_b^j s_{ij}^{ab} \\
&+ \frac{1}{2} \sum_{jbc} g_{bc}^{aj} s_{ij}^{bc} - \frac{1}{2} \sum_{jkb} g_{ib}^{jk} s_{jk}^{ab} + \sum_{jkbc} g_{bc}^{jk} s_j^b s_{ki}^{ca} \\
&- \frac{1}{2} \sum_{jkbc} g_{bc}^{jk} s_i^b s_{jk}^{ac} - \frac{1}{2} \sum_{jkbc} g_{bc}^{jk} s_j^a s_{ik}^{bc} \ ,
\end{aligned} \tag{34}$$

respectively. Note that in each term a cancellation of the indices from top to bottom

yields some result Z_i^a, which can contribute to $\overline{H}_i^a$.

The diagrams which contribute to the element $\left\langle \Phi_{ij}^{ab} \right| \overline{H}_S \left| \Phi \right\rangle \equiv \overline{H}_{ij}^{ab}$, which appears on the right-hand side of Eq. (31), must have two pairs of external lines ($a_a^\dagger$,a_i) and ($a_b^\dagger$,a_j). Since in this case the number of possibilities is relatively extensive, I divide the various contributions to $\overline{H}_{ij}^{ab}$ between two figures: Figs. 5 and 6 contain the diagrams with and without S_1 vertices, respectively. Note the diagrammatic representation of the element $\overline{H}_{ij}^{ab}$ on the left-hand sides of the figures.

The algebraic expressions associated with the diagrams in Figs. 5 and 6 are given by

$$
\begin{aligned}
\overline{H}_{ij}^{ab} \;=\;& P(ij) \sum_c g_{cj}^{ab} s_i^c - P(ab) \sum_k g_{ij}^{kb} s_k^a + \sum_{cd} g_{cd}^{ab} s_i^c s_j^d \\
&+ \sum_{kl} g_{ij}^{kl} s_k^a s_l^b - P(ij|ab) \sum_{kc} g_{cj}^{kb} s_i^c s_k^a + P(ij) \sum_{klc} g_{cj}^{kl} s_i^c s_k^a s_l^b \\
&- P(ab) \sum_{kcd} g_{cd}^{kb} s_i^c s_k^a s_j^d - P(ij) \sum_{kc} f_c^k s_i^c s_{kj}^{ab} - P(ab) \sum_{kc} f_c^k s_k^a s_{ij}^{cb} \\
&- \frac{1}{2} P(ab) \sum_{kcd} g_{cd}^{kb} s_k^a s_{ij}^{cd} + \frac{1}{2} P(ij) \sum_{klc} g_{cj}^{kl} s_i^c s_{kl}^{ab} + \sum_{klcd} g_{cd}^{kl} s_i^c s_k^a s_l^b s_j^d \\
&- P(ij) \sum_{klc} g_{ci}^{kl} s_k^c s_{lj}^{ab} + P(ab) \sum_{kcd} g_{cd}^{ka} s_k^c s_{ij}^{db} + P(ij|ab) \sum_{kcd} g_{cd}^{ak} s_i^c s_{kj}^{db} \\
&- P(ij|ab) \sum_{klc} g_{ic}^{kl} s_k^a s_{lj}^{cb} - P(ij|ab) \sum_{klcd} g_{cd}^{kl} s_i^c s_k^a s_{lj}^{db} + \frac{1}{2} \sum_{klcd} g_{cd}^{kl} s_i^c s_{kl}^{ab} s_j^d \\
&+ \frac{1}{2} \sum_{klcd} g_{cd}^{kl} s_k^a s_{ij}^{cd} s_l^b - P(ab) \sum_{klcd} g_{cd}^{kl} s_k^c s_l^a s_{ij}^{db} - P(ij) \sum_{klcd} g_{cd}^{kl} s_k^c s_i^d s_{lj}^{ab} \\
&+ g_{ij}^{ab} + P(ab) \sum_c f_c^b s_{ij}^{ac} - P(ij) \sum_k f_j^k s_{ik}^{ab} + \frac{1}{2} \sum_{cd} g_{cd}^{ab} s_{ij}^{cd} \\
&+ \frac{1}{2} \sum_{kl} g_{ij}^{kl} s_{kl}^{ab} + P(ij|ab) \sum_{kc} g_{cj}^{kb} s_{ik}^{ac} - \frac{1}{2} P(ij) \sum_{klcd} g_{cd}^{kl} s_{ki}^{cd} s_{lj}^{ab} \\
&- \frac{1}{2} P(ab) \sum_{klcd} g_{cd}^{kl} s_{kl}^{ca} s_{ij}^{db} + P(ij) \sum_{klcd} g_{cd}^{kl} s_{ik}^{ac} s_{lj}^{db} + \frac{1}{4} \sum_{klcd} g_{cd}^{kl} s_{ij}^{cd} s_{kl}^{ab} \;,
\end{aligned}
\tag{35}
$$

where the terms are ordered from left to right, row by row, in the order in which the corresponding diagrams are presented in the figures. Note in Eq. (35) that permutations are generated by the operator $P(pq)$, whereby $P(pq)f(pq) \equiv f(pq) - f(qp)$. Thus dual permutations are generated as $P(pq|rs)f(pqrs) \equiv f(pqrs) - f(qprs) -$

$f(pqsr) + f(qpsr)$. Again, a cancellation of indices from top to bottom in each term reveals a contribution Z_{ij}^{ab} to the element $\overline{H}_{ij}^{ab}$.

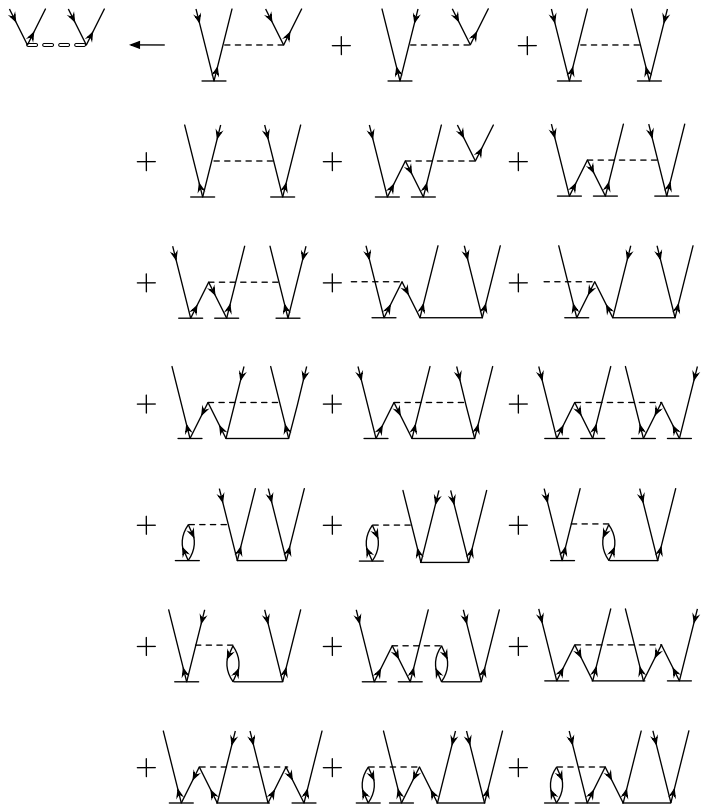

Figure 5. Contributions to the element $\overline{H}_{ij}^{ab}$ containing at least one S_1 vertex.

At this point, the equations governing the time-evolution of the excitation amplitudes s_0, s_i^a, and s_{ij}^{ab}—for which abridged representations are given by Eqs. (29)-(31)—are completely determined. It is clear from the expansions of the elements $\overline{H}_0$, $\overline{H}_i^a$, and $\overline{H}_{ij}^{ab}$, given in Eqs. (33)-(35), that Eqs. (29)-(31) are linear in the matrix elements of the two-body Hamiltonian and nonlinear in the excitation amplitudes. Note also that, though the equations are coupled in the amplitudes s_i^a and s_{ij}^{ab}, Eqs. (30) and (31) are independent of the complex phase s_0. For this reason, it is customary to neglect s_0—thus the integration of Eq. (29)—within calculations [18]; and I have

done so in this work.

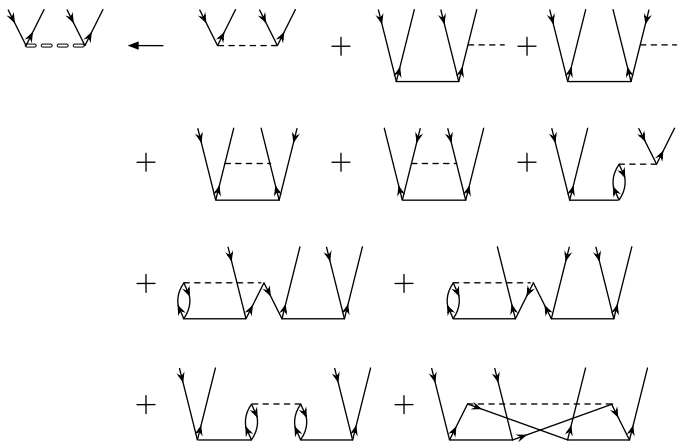

Figure 6. Contributions to the element $\overline{H}^{ab}_{ij}$ containing no S_1 vertices.

It is instructive to rewrite Eqs. (29)-(31) in operator form. Within a Hilbert space which includes up to $2p$-$2h$ excited states, the similarity-transformed Hamiltonian $\overline{H}_S$ can be represented in 3x3 block form as

$$\overline{H}_S \;=\; \begin{pmatrix} \langle\Phi|\,\overline{H}_S\,|\Phi\rangle & \langle\Phi|\,\overline{H}_S\,|\Phi^c_k\rangle & \langle\Phi|\,\overline{H}_S\,\big|\Phi^{cd}_{kl}\big\rangle \\ \langle\Phi^a_i|\,\overline{H}_S\,|\Phi\rangle & \langle\Phi^a_i|\,\overline{H}_S\,|\Phi^c_k\rangle & \langle\Phi^a_i|\,\overline{H}_S\,\big|\Phi^{cd}_{kl}\big\rangle \\ \big\langle\Phi^{ab}_{ij}\big|\,\overline{H}_S\,|\Phi\rangle & \big\langle\Phi^{ab}_{ij}\big|\,\overline{H}_S\,|\Phi^c_k\rangle & \big\langle\Phi^{ab}_{ij}\big|\,\overline{H}_S\,\big|\Phi^{cd}_{kl}\big\rangle \end{pmatrix} \;; \tag{36}$$

thus Eqs. (29)-(31) can be written more-concisely as

$$i\hbar\dot{S} \;=\; \overline{H}_{S_1}\;, \tag{37}$$

where $\overline{H}_{S_1}$ is representative of the $\overline{H}_S$ matrix when all elements but those in the first column of the block form are set to zero.

The Λ amplitude equations

To re-derive equations that govern the time-evolution of the de-excitation amplitudes λ^i_a and λ^{ij}_{ab}, we use the form of the left many-body wavefunction given in

Eq. (16) and right-multiply the time-dependent Schrödinger equation [see Eq. (8)] by the cluster operator e^S, such that

$$-i\hbar \langle \Phi | \Lambda e^{-S} \partial_t e^S = \langle \Phi | \Lambda \overline{H}_S \ . \tag{38}$$

Then, making the substitutions $e^{-S}\partial_t e^S = \partial_t - \dot{S}$ [see Eq. (28]—since, within a time-independent basis, the commutator $[\dot{S}, S]$ does not contribute here—and $\dot{S} = -\frac{i}{\hbar}\overline{H}_{S_1}$ [see Eq. (37)] and left-projecting with the states $|\Phi_i^a\rangle$ and $|\Phi_{ij}^{ab}\rangle$, we obtain the component expressions

$$-i\hbar \dot{\lambda}_a^i = \langle \Phi | \Lambda \left(\overline{H}_S - \overline{H}_{S_1} \right) | \Phi_i^a \rangle \tag{39}$$

$$-i\hbar \dot{\lambda}_{ab}^{ij} = \langle \Phi | \Lambda \left(\overline{H}_S - \overline{H}_{S_1} \right) | \Phi_{ij}^{ab} \rangle \tag{40}$$

for which the concise, operator form can be written as

$$-i\hbar \dot{\Lambda} = \Lambda \left(\overline{H}_S - \overline{H}_{S_1} \right) \ . \tag{41}$$

According to Eqs. (39) and (40), contributing to the first-order time derivative of the de-excitation amplitudes λ_a^i and λ_{ab}^{ij} are all such diagrams that contain one pair of external lines $(a_i^\dagger, a_a)$ and two pairs of external lines $(a_i^\dagger a_a)$ and $(a_j^\dagger a_b)$, respectively, and that are furthermore formed by the connection of a Λ fragment with any element of $\overline{H}_S$ that is not in the first column of its block form [see Eq. (36)]. Without further explanation, Figs. 7 and 8 contain the diagrammatic forms of the right-hand sides of Eqs. (39) and (40), respectively. Note several things from the figures. First, the λ_a^i and λ_{ab}^{ij} fragments are inverted relative to s_a^i and s_{ab}^{ij} fragments, and I have illustrated them with thick lines [see Fig. 27]. Second, due to the linearity of Λ [see Eq. (17)], no diagram contains more than one Λ fragment. This restriction is quite important since it clearly limits the number of contributions to the expressions. Consider an alternative: if, for example, $\Lambda \to e^\Lambda$, the number of contributions would be much larger since the number of Λ fragments per contribution could be greater than one. Third, unlike the diagrams shown in Figs. 3-6, which each contribute to specific elements of

$\overline{H}_S$—namely, $\overline{H}_0$, $\overline{H}_i^a$, and $\overline{H}_{ij}^{ab}$—the diagrams in Figs. 7 and 8 are written in terms of the various elements of $\overline{H}_S$, whose diagram fragments are illustrated with thick dotted lines in the figures. Because these elements appear as intermediate quantities throughout coupled-cluster theory, I provide their diagrammatic and algebraic expansions in Appendix D. Fourth, in the figures, note the dependence on a few three-body terms of $\overline{H}_S$: despite the fact that H_N is a two-body Hamiltonian, its e^S-mediated similarity-transformation yields in fact up to six-body terms in $\overline{H}_S$ within the CCSD approximation [49]; however, due to the linear nature of Λ and the CCSD restriction to only λ_a^i and λ_{ab}^{ij}, no contributions to the elements $\langle\Phi|\,\Lambda\left(\overline{H}_S-\overline{H}_{S_1}\right)|\Phi_i^a\rangle$ and $\langle\Phi|\,\Lambda\left(\overline{H}_S-\overline{H}_{S_1}\right)|\Phi_{ij}^{ab}\rangle$ can be generated from the N-body terms, $N\geq 4$, of $\overline{H}_S$. Finally, note that the second diagram in Fig. 8 is *disconnected*—i.e., it contains no internal lines. It appears in the expansion since, unlike the diagrams associated with Eqs. (29)-(31), each of which must contain at least one internal line according to Eq. (27) and is thus deemed *connected*, there is no such connectedness condition for Eqs. (39) and (40).

The algebraic interpretations of the diagrams in Figs. 7 and 8 are given by

$$\begin{aligned}
-i\hbar\dot{\lambda}_a^i &= \overline{H}_a^i+\sum_b \overline{H}_a^b\lambda_b^i-\sum_j \overline{H}_j^i\lambda_a^j+\sum_{jb}\overline{H}_{aj}^{ib}\lambda_b^j \\
&\quad+\frac{1}{2}\sum_{jbc}\overline{H}_{aj}^{bc}\lambda_{bc}^{ij}-\frac{1}{2}\sum_{jkb}\overline{H}_{jk}^{ib}\lambda_{ab}^{jk}+\sum_{jkbc}\overline{H}_{ajk}^{ibc}\lambda_{bc}^{jk} \qquad (42)\\
-i\hbar\dot{\lambda}_{ab}^{ij} &= \overline{H}_{ab}^{ij}+P(ab|ij)\overline{H}_b^j\lambda_a^i+P(ij)\sum_c\overline{H}_{ab}^{cj}\lambda_c^i-P(ab)\sum_k\overline{H}_{kb}^{ij}\lambda_a^k \qquad (43)\\
&\quad+P(ab)\sum_c\overline{H}_b^c\lambda_{ac}^{ij}-P(ij)\sum_k\overline{H}_k^j\lambda_{ab}^{ik}+P(ab|ij)\sum_{kc}\overline{H}_{ak}^{ic}\lambda_{cb}^{kj}\\
&\quad+\frac{1}{2}\sum_{cd}\overline{H}_{ab}^{cd}\lambda_{cd}^{ij}+\frac{1}{2}\sum_{kl}\overline{H}_{kl}^{ij}\lambda_{ab}^{kl}+\frac{1}{2}P(ij)\sum_{kcd}\overline{H}_{akb}^{cdj}\lambda_{cd}^{ik}\\
&\quad-\frac{1}{2}P(ab)\sum_{klc}\overline{H}_{klb}^{icj}\lambda_{ac}^{kl}\,,
\end{aligned}$$

respectively. If desired, these equations may instead be written in terms of the S amplitudes and the one-body and two-body interactions F_N and G_N by substitution

of the expressions corresponding to the $\overline{H}_S$ intermediates [see Appendix D]. Such a substitution makes it clear that Eqs. (37) and (41) are coupled only in the S amplitudes.

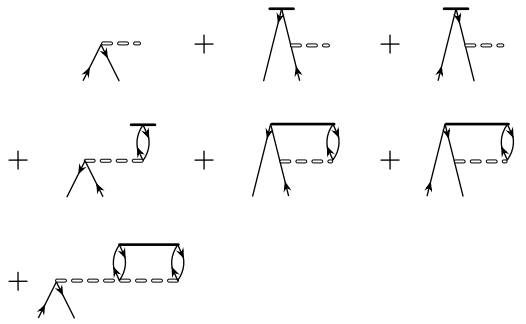

Figure 7. Diagrammatic expansion of $\langle\Phi|\,\Lambda\left(\overline{H}_S - \overline{H}_{S_1}\right)|\Phi_i^a\rangle$.

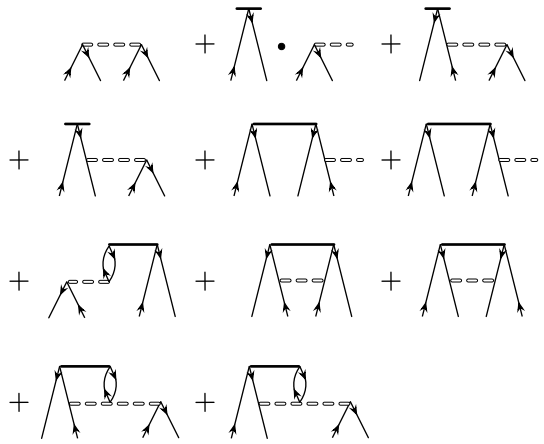

Figure 8. Diagrammatic expansion of $\langle\Phi|\,\Lambda\left(\overline{H}_S - \overline{H}_{S_1}\right)|\Phi_{ij}^{ab}\rangle$.

Together, Eqs. (37) and (41) constitute the TD-CCSD equations: considering the parameterizations of the right and left many-body wavefunctions [see Eqs. (9) and (16)], the step-wise, simultaneous solution of the component equations—Eqs. (30), (31), (39), and (40)—is all that is needed to implement the theory within a time-independent basis [31].

Observables

We are now equipped to check that the energy functional [see Eq. (18)] is indeed conserved in time:

$$\begin{aligned}\dot{\mathbb{E}} &= \langle\Phi|\left(\dot{\Lambda}\overline{H}_S + \Lambda\dot{\overline{H}}_S\right)|\Phi\rangle \\ &= \frac{i}{\hbar}\langle\Phi|\,\Lambda\big(\overline{H}_S\overline{H}_S - \overline{H}_{S_1}\overline{H}_S - \overline{H}_S\overline{H}_{S_1} + \overline{H}_{S_1}\overline{H}_S\big)|\Phi\rangle \\ &= 0\ , \end{aligned} \tag{44}$$

which relies on the following: $\dot{H} = 0$; Eq. (41); and the identities $\dot{\overline{H}}_S = [\overline{H}_S, \dot{S}] = -\frac{i}{\hbar}[\overline{H}_S, \overline{H}_{S_1}]$ and $\overline{H}_S|\Phi\rangle = \overline{H}_{S_1}|\Phi\rangle$. While the latter identity is evident from Eq. (36), the former identity is easily shown:

$$\begin{aligned}\dot{\overline{H}}_S &\equiv \partial_t\big(e^{-S}H_N e^S\big) \\ &= -\dot{S}\overline{H}_S + e^{-S}\dot{H}_N e^S + \overline{H}_S\dot{S} \\ &= [\overline{H}_S, \dot{S}] \\ &= -\frac{i}{\hbar}[\overline{H}_S, \overline{H}_{S_1}]\ , \end{aligned} \tag{45}$$

where I have used Eq. (37) in the last equality. Here it is quite important to note that all of the identities used to arrive at the result in Eq. (44) also hold when the theory is formulated in terms of imaginary time $\tau \equiv it$ (discussed at length in the following chapter); thus $\partial_\tau\mathbb{E} = 0$. Therefore, the functional $\mathbb{E}$ is complex-analytic in time: it is conserved in any time domain.

For the computation of the energy functional, I provide the diagrammatic expansion of its correlation correction $\Delta\mathbb{E} \equiv \langle\Phi|\,\Lambda\overline{H}_S|\Phi\rangle$ in Fig. 9. From the figure, note that $\Delta\mathbb{E}$ contains all of the closed-diagram contributions of the product $\Lambda\overline{H}_S$. Specifically, the first three diagrams constitute the element $\overline{H}_0$ while the last two diagrams are representative of the contractions $\langle\Phi|\,\overbrace{\Lambda_1\overline{H}_S}\,|\Phi\rangle$ and $\langle\Phi|\,\overbrace{\Lambda_2\overline{H}_S}\,|\Phi\rangle$, where Λ_1 and Λ_2 are the second and third terms in Eq. (17). The algebraic expansion of

the total value of the functional is then given as

$$\mathbb{E} \;=\; \langle\Phi|\, H\,|\Phi\rangle + \overline{H}_0 + \sum_{ia} \overline{H}_i^a \lambda_a^i + \frac{1}{4}\sum_{ijab} \overline{H}_{ij}^{ab} \lambda_{ab}^{ij}\;, \tag{46}$$

where the expansion of the reference energy $\langle\Phi|\, H\,|\Phi\rangle$ is provided in Eq. (23), and the remaining terms are given in the order in which their corresponding diagrams appear in Fig. 9. As is shown in the next subsection, the first two terms of Eq. (46) $\langle\Phi|\, H\,|\Phi\rangle + \overline{H}_0$ constitute the CCSD ground-state energy E_{CCSD} provided that the elements $\overline{H}_i^a = 0 = \overline{H}_{ij}^{ab}$. Therefore $\mathbb{E}$ may in fact be interpreted as an optimized Lagrange functional subject to these constraints:

$$\mathbb{E} \;=\; E_{CCSD}(S(t)) + \Lambda_a^i\Big(\overline{H}_i^a(S(t)) \pm 0\Big) + \Lambda_{ab}^{ij}\Big(\overline{H}_{ij}^{ab}(S(t)) \pm 0\Big)\;, \tag{47}$$

whereby the component amplitudes λ_a^i and λ_{ab}^{ij} serve as Lagrange multipliers [50]. This implies that $\mathbb{E}$ is a stationary, thus variational (in fact, bi-variational, due to the non-Hermitian quality of $\overline{H}$) functional, since even in cases where the elements $\overline{H}_i^a$ and $\overline{H}_{ij}^{ab}$ are non-trivial—i.e., when the amplitudes s_i^a and s_{ij}^{ab} have a non-trivial time evolution, $\mathbb{E}$ is the appropriate energy. To my knowledge, such a connection was first made by H. Koch and J. Jørgensen in the context of coupled-cluster linear response methods [26].

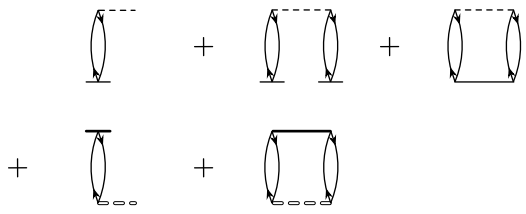

Figure 9. Diagrammatic expansion of $\Delta\mathbb{E} = \langle\Phi|\, \Lambda\overline{H}_S\,|\Phi\rangle$.

In addition to the energy functional, any observable which commutes with the Hamiltonian must be conserved. Note that any operator O that commutes with

the true Hamiltonian—$[H, O] = 0$—also commutes with the effective Hamiltonian—$[\overline{H}, \overline{O}] = 0$. Considering the parameterizations given in Eqs. (9) and (16), the expectation value of an observable O is given as

$$\langle O \rangle \;=\; \langle \Phi | \, \Lambda e^{-S} O e^{S} \, | \Phi \rangle \;\equiv\; \langle \Phi | \, \Lambda \overline{O} \, | \Phi \rangle \;. \tag{48}$$

Then, if $[H, O] = 0$, the time derivative $\langle \dot{O} \rangle$ is given by

$$\begin{aligned} \langle \dot{O} \rangle &= \langle \Phi | \left(\dot{\Lambda} \overline{O} + \Lambda \dot{\overline{O}} \right) | \Phi \rangle \\ &= \frac{i}{\hbar} \langle \Phi | \, \Lambda \big(\overline{HO} - \overline{H}_1 \overline{O} + \overline{H}_1 \overline{O} - \overline{OH} \big) \, | \Phi \rangle \\ &= \frac{i}{\hbar} \langle \Phi | \, \Lambda [\overline{H}, \overline{O}] \, | \Phi \rangle \\ &= 0 \;, \end{aligned} \tag{49}$$

where I have used the following: $\dot{H} = 0 \Rightarrow \dot{O} = 0 \Leftrightarrow [H, O] = 0$; Eq. (41); the identity $\dot{\overline{O}} = [\overline{O}, \dot{S}] = \frac{i}{\hbar} [\overline{H}_1, \overline{O}]$, a straightforward generalization of Eq. (45); and, again, the fact that $\overline{H}_1 \, | \Phi \rangle = \overline{H} \, | \Phi \rangle$.

For the computation of an observable, one typically utilizes density matrices. In the coupled-cluster formalism, the normal-ordered one-body and two-body density matrices are given by

$$(\rho^q_p)_N \;\equiv\; \langle \Phi | \, \Lambda e^{-S} \{ p^\dagger q \} e^{S} \, | \Phi \rangle \tag{50}$$

$$(\rho^{rs}_{pq})_N \;\equiv\; \langle \Phi | \, \Lambda e^{-S} \{ p^\dagger q^\dagger s r \} e^{S} \, | \Phi \rangle \tag{51}$$

and are used to find the correlation correction to the expectation value of any one-body or two-body observable. (For an n-body observable, $n > 2$, it is of course necessary to also consider m-body densities, $m = 3, \ldots, n$.) For example, the expectation value of a one-body operator O can be written as

$$\langle O \rangle \;=\; \sum_{pq} O^p_q \, \langle \tilde{\Psi} | \, \{ p^\dagger q \} \, | \Psi \rangle + \langle \Phi | \, O \, | \Phi \rangle \;, \tag{52}$$

where $\{ \langle \tilde{\Psi} | \, , | \Psi \rangle \}$ and $| \Phi \rangle$ are the correlated and uncorrelated (reference) wavefunctions. The second term in Eq. (52) is the reference expectation value of O and is thus

computed simply by summing over the elements along its diagonal—i.e., $\sum_i O_i^i$. For this reason, the first term in Eq. (52), which clearly contains the contribution of the correlations induced within the many-body method used, is the term of interest. In the coupled-cluster formalism, it is written in accordance with Eq. (50) as

$$\langle O_N \rangle \;=\; \sum_{pq} O_q^p \, \langle \Phi | \, \Lambda e^{-S} \{ p^\dagger q \} e^S \, | \Phi \rangle \;=\; \sum_{pq} O_q^p (\rho_p^q)_N \; . \tag{53}$$

In a similar way, the correlation correction to the expectation value of a two-body operator T can be written in terms of both the normal-ordered one-body and two-body densities:

$$\langle T_N \rangle \;=\; \frac{1}{4} \sum_{pqrs} T_{rs}^{pq} (\rho_{pq}^{rs})_N + \sum_{pq} \tilde{T}_q^p (\rho_p^q)_N \; , \tag{54}$$

where $\tilde{T}_q^p = \sum_i T_{qi}^{pi}$ can be construed as the "effective" one-body elements of T.

For completeness, I provide the diagrammatic and algebraic expansions of the normal-ordered one-body and two-body densities in Appendix E. Note that the expansions are finite due to the linearity of Λ [see Eq. (17)]; thus it is now quite clear that the expectation value of any observable can be expressed exactly within the bi-variational coupled-cluster formalism.

Time-Independent Coupled-Cluster Theory

It is important that the time-independent CCSD (TI-CCSD) equations are recovered from Eqs. (29)-(31) in the time-independent limit. (For the standard derivation of the TI-CCSD equations, see the article by T. Crawford and H. Schaefer [37].) Such a deduction is straightforward: in the limit that the excitation amplitudes s_i^a and s_{ij}^{ab} do not depend on time, Eqs. (30) and (31) become

$$\langle \Phi_i^a | \, \overline{H}_S \, | \Phi \rangle \;=\; 0 \tag{55}$$

$$\left\langle \Phi_{ij}^{ab} \right| \overline{H}_S \, | \Phi \rangle \;=\; 0 \; , \tag{56}$$

which is indicative that the reference state $|\Phi\rangle$ is an eigenstate of $\overline{H}$ within the basis of $1p$-$1h$ and $2p$-$2h$ excited states. Furthermore, it is clear from Eqs. (46), (55), and (56) that the corresponding eigenvalue is given by

$$\begin{aligned} E_{CCSD} &= \langle\Phi|\, H\, |\Phi\rangle + \overline{H}_0 \\ &= \langle\Phi|\, (H + \overline{H}_S)\, |\Phi\rangle \\ &= \langle\Phi|\, \overline{H}\, |\Phi\rangle \ . \end{aligned} \tag{57}$$

Eqs. (55) and (56) are indeed the TI-CCSD equations. Together with Eq. (57), they indicate that the element $\overline{H}_0$ is the CCSD ground-state correlation energy provided that the S amplitudes take on values such that $\overline{H}_S$ does not correlate the reference and excited states.

Additionally, Eqs. (57) and (29) imply that the $0p$-$0h$ phase s_0 is given by

$$s_0 = C - \frac{i}{\hbar}\overline{H}_0 t, \tag{58}$$

where C is a constant to be determined.

Note that the coupled-cluster energy functional $\mathbb{E}$ [see Eq. (46)] is equivalent to $\langle\Phi|\, \overline{H}\, |\Phi\rangle$ only if Eqs. (55) and (56) hold; thus in the time-dependent case, when the amplitudes acquire a non-trivial time evolution according to Eqs. (30) and (31), the element $\overline{H}_0$ is *not* an energy. This is an insight recently-illustrated [29] and one that will be addressed in the following chapter.

Coupled-Cluster Equations of Motion

The coupled-cluster equations of motion, used frequently within computations of nuclear excited states and excited-state properties [38, 40] and to extend coupled-cluster computations into the domain of open-shell nuclei [51,52], may also be deduced from the TD-CC equations. Since the equations of motion are used throughout many

of the applications in Chapter 3, I provide a short overview of the standard formalism prior to making the deduction. Here I consider the equations in the CCSD approximation.

In short, consider some state $|\Psi_q\rangle = R_q |\Psi\rangle$, where the operator R_q is a linear excitation operator having the same form as S [see Eq. (10)] and $|\Psi\rangle$ is parameterized as in Eq. (9). Then, when the TI-CCSD equations [see Eqs. (55) and (56)] have been solved, the time-independent Schrödinger equation reads

$$\overline{H}_T R_q |\Phi\rangle \;=\; \Delta E_q R_q |\Phi\rangle \;, \tag{59}$$

where $\overline{H}_T \equiv e^{-T} H_N e^T$ and $S = T$ solves the TI-CCSD equations, and I have used the fact that $[R, S] = 0 \therefore [R, e^S] = 0$. It is clear from Eq. (59) that the state $R_q |\Phi\rangle$ is the q-th eigenstate of $\overline{H}$ with a correlation energy given by ΔE_q. Furthermore, since the TI-CCSD equations are satisfied, the reference state $|\Phi\rangle$ is itself the CCSD ground-state, with correlation $\Delta E_0 = \overline{H}_0$ [see Eq. (57)]. Thus Eq. (59) provides the starting point for studying nuclear excited states within the coupled-cluster formalism.

If we multiply the ground-state Schrödinger equation $\overline{H}_T |\Phi\rangle = \Delta E_0 |\Phi\rangle$ by R_q, subtract it from Eq. (59), and left-project with the states $\langle\Phi|$, $\langle\Phi_i^a|$, and $\langle\Phi_{ij}^{ab}|$, we obtain equations for the R_q amplitudes:

$$\langle\Phi| [\overline{H}_T, R] |\Phi\rangle \;=\; \omega r_0 \tag{60}$$

$$\langle\Phi_i^a| [\overline{H}_T, R] |\Phi\rangle \;=\; \omega r_i^a \tag{61}$$

$$\langle\Phi_{ij}^{ab}| [\overline{H}_T, R] |\Phi\rangle \;=\; \omega r_{ij}^{ab} \;, \tag{62}$$

where $\omega = \Delta E - \Delta E_0$ and I have dropped the subscript q to simplify notation. Note that Eqs. (60)-(62) constitute the appropriate "matrix-vector" operations needed within the iterative solution of Eq. (59)—i.e., such as in Arnoldi [53] or Lanczos approaches. Succinctly, Eqs. (60)-(62) may be expressed as

$$\overline{\overline{H}_T R} \;=\; \omega R \;, \tag{63}$$

wherein it has been deduced from Eqs. (26) and (27) that $[\overline{H}_T, R] \rightarrow \overline{H}_T R$.

In a similar way, we could derive working equations for the left eigenvalue problem of $\overline{H}$,

$$\langle \Phi | \, L_q \overline{H}_T \;\; = \;\; \langle \Phi | \, L_q \Delta E_q \; , \tag{64}$$

where L_q is a linear de-excitation operator having the same form as Λ [see Eq. (17)] with the exception that the first term l_0 is not necessarily equivalent to 1. Skipping the details, the equations for the L_q amplitudes are

$$\langle \Phi | \, [L, \overline{H}_T] \, | \Phi \rangle \;\; = \;\; \omega l_0 \tag{65}$$

$$\langle \Phi | \, [L, \overline{H}_T] \, | \Phi_i^a \rangle \;\; = \;\; \omega l_a^i \tag{66}$$

$$\langle \Phi | \, [L, \overline{H}_T] \, | \Phi_{ij}^{ab} \rangle \;\; = \;\; \omega l_{ab}^{ij} \; , \tag{67}$$

where again the subscript q is suppressed. These equations may be written concisely as

$$[L, \overline{H}_T] \;\; = \;\; \omega L \; . \tag{68}$$

Note that a contraction such as that in Eq. (63) is not present here since, like the Λ equations [see Eqs. (39) and (40)], the L equations are not limited to connected contributions.

Eqs. (60)-(62) and (65)-(67) are the "right" and "left" equations of motion in the CCSD approximation (EOM-CCSD equations). Since I use the equations within applications, I provide the associated diagrammatic and algebraic expansions in Appendix F.

Since $\overline{H}$ is non-Hermitian, the eigenstates $\langle \tilde{\Phi}_p | \equiv \langle \Phi | \, L_p$ and $| \Phi_q \rangle \equiv R_q \, | \Phi \rangle$ form a biorthogonal set, such that $\langle \tilde{\Phi}_p | \Phi_q \rangle = \delta_q^p$. Furthermore, since the left and right eigenvalues are identical, it is only necessary to solve both Eqs. (59) and (64) within a study of excited-state properties other than energy. For this purpose, the normal-

ordered one-body and two-body densities for the z-th excited state are written as

$$(\rho_p^q)_N^z \equiv \langle\Phi|\, L_z e^{-S}\{p^\dagger q\}e^S R_z\,|\Phi\rangle \tag{69}$$

$$(\rho_{pq}^{rs})_N^z \equiv \langle\Phi|\, L_z e^{-S}\{p^\dagger q^\dagger sr\}e^S R_z\,|\Phi\rangle\ . \tag{70}$$

Note that the diagrammatic contributions to these densities are somewhat similar to those of the densities in Eqs. (50) and (51) [see Appendix E] but differ primarily in the addition of R vertices. Only in the ground-state, where $R_0 = r_0 = 1$, are the densities identical. Since the densities in Eqs. (69) and (70) are not employed within the applications discussed in the following chapter, I refer the interested reader to the renowned article by J. Stanton and R. J. Bartlett [38] for the associated diagrammatic and algebraic expansions.

We can in fact derive Eqs. (61) and (62) from within the time-dependent formalism. If we neglect the $0p$-$0h$ amplitudes s_0 and r_0, such that $\tilde{S} \equiv \{s_i^a, s_{ij}^{ab}\}$ and $\tilde{R} \equiv \{r_i^a, r_{ij}^{ab}\}$, and substitute into Eq. (37) the ansatz $\tilde{S}(t) = \tilde{T} + \tilde{R}(t)$, whereby $\tilde{S} = \tilde{T}$ solves the TI-CCSD equations, assuming that $|\tilde{R}| \ll |\tilde{T}|$, we obtain straightaway

$$i\hbar\dot{\tilde{R}} = \overline{H}_{\tilde{T}} + [\overline{H}_{\tilde{T}}, \tilde{R}] \tag{71}$$

to first order. Furthermore, if we assume a simple harmonic time dependence, such that $\tilde{R}(t) = \tilde{R}e^{-i\omega t}$, it is clear that the amplitudes r_i^a and r_{ij}^{ab} are indeed given by Eqs. (61) and (62). Note that, in the deduction of Eq. (71), the $0p$-$0h$ amplitude r_0 can be neglected since, like s_0 [see Eq. (58)], r_0 must have a trivial time dependence. Furthermore, due to dependence on the commutation $[\overline{H}_T, R]$, Eqs. (60)-(62) are coupled only in r_i^a and r_{ij}^{ab}; therefore, r_0 is determined by Eq. (60) only after the amplitudes r_i^a and r_{ij}^{ab} have been determined by Eqs. (61) and (62). Recall from the last subsection that the TI-CCSD equations [see Eqs. (55) and (56)] are energy-independent, and the energy is determined by Eq. (57) only after they have been solved. The analogy here is no coincidence: Eqs. (60)-(62) are merely manipulations

of Eqs. (57), (55), and (56) whereby the commutations leave behind only the R amplitudes.

Starting with Eq. (41), we could derive Eqs. (66) and (67) in a similar way.

Though we have followed the traditional, time-independent approach, whereby $S = T$, in the derivation of the EOM-CCSD equations—it is clear that the equations can be tailored to the general case, whereby $S \neq T$. (Therefore $\overline{H}_T \rightarrow \overline{H}_S$ in the equations.) This provides a venue for studying the time-evolution of observables: one can time-evolve the S amplitudes according to Eq. (37) and periodically solve the right or left EOM-CCSD equations—or both, in the case that one wants to compute the density matrices [see Eqs. (69) and (70)] and track observables aside to energy. Since the EOM-CCSD equations are independent of Λ, the Λ amplitudes can be neglected during the computation. As I will exemplify in the following chapter, this method has the disadvantage that the Hilbert space in which the diagonalization of $\overline{H}$ is done is restricted to the $2p$-$2h$ level and is thus inexact when applied to systems containing more than two particles. And, though one can certainly do the calculation within a larger space, the computational effort required to do so is substantially greater. As an example, an EOM-CCSDT computation, which incorporates up to $3p$-$3h$ excited states, has more than twice the computational requirement of an EOM-CCSD computation. For this reason, it is desirable to adhere to bi-variational TD-CC [see Eqs. (37), (41), (18), (50), and (51)] for the computation of observables.

CHAPTER III

APPLICATIONS

Initial applications of TD-CC to study some intrinsic properties of atomic nuclei and two-level Lipkin systems are discussed. Though in many cases "I" and "my" are used in order to distinguish actions that have occurred apart from the reader, note that much of this work has been done with guidance and insight provided by the coauthors of Ref. [36]. Also, when it is said that "I solve the [...] equations," it is understood that this has been done via a computational implementation of codes which I have authored.

Specifically, to establish both the validity of my implementation of TD-CC theory and its usefulness in regard to the nuclear many-body problem, I revisit the computation done by P. Hoodbhoy and J. W. Negele [19] of the excitation energy of interacting Lipkin systems [20] as a function of the time over which the systems have interacted; observe the expectation value of the one-body interaction as a function of time for a single Lipkin system; conduct a Fourier analysis of time-evolved S amplitudes, from which nuclear excited state energies can be obtained, and compare results with those obtained separately by solving the EOM-CC equations in the time-independent formalism; and present a comprehensive study of the real-time and imaginary-time evolutions of energy for nuclei, confirming that the bi-variational formulation [31] of TD-CC conserves energy quite well while discovering that the time-evolution of the eigenvalues of $\overline{H}$ is instead more useful within the imaginary-time suppression of excitations. Throughout, unless otherwise specified, I use the CCSD approximation.

In those applications involving the computation of nuclear properties, I employ a low-momentum, two-body Hamiltonian obtained from a similarity renormalization group (SRG) transformation [54] of the N^{3}LO interaction from chiral effective field

theory [55], using the cutoff $\Lambda = 1.9$ fm^{-1}, which corresponds to a peak momentum of roughly 375 MeV/c ($\hbar c \approx 197$ MeV fm)—i.e., well-below the threshold for having quark and gluon degrees of freedom ($\approx$ 1 GeV). Furthermore, for computational efficiency, I use a model space of only four oscillator shells—i.e., up to the second p-1/2 level and thus including a total of forty proton and forty neutron states. Such a small model space is sufficient here, since the primary goal throughout is to demonstrate the practicality of TD-CC as a nuclear many-body method by doing proof-of-principle calculations. However, for comparison with experimental data, it is understood that a model space of significantly-greater size would be required.

For the time integrations of the S and Λ amplitudes according to Eqs. (37) and (41), I use the well-known fourth-order Runge-Kutta method (RK4) [56]. Note that techniques which involve adaptive step sizes, such as adaptive RK4 or the Bulirsch-Stoer method [57], are not especially useful here since, as I have discovered, the amplitudes can vary quite rapidly with time, depending on the system studied. Thus such methods are rendered less precise unless they are formulated at higher-order, and in those cases they are in fact computationally less-efficient than RK4 with a small, constant step size.

In a number of cases, I begin by solving the TI-CCSD equations [see Eqs. (55) and (56)] in order to obtain the ground-state wavefunction and then perturb the S amplitudes by small random values prior to time-evolving. Note that the perturbations to S are essential, since, if the TI-CCSD equations are exactly-solved ($\overline{H}_i^a = 0 = \overline{H}_{ij}^{ab}$), the S amplitudes are rendered constants according to Eqs. (30) and (31). The Λ amplitudes, however, need no perturbation: though they are identically-zero in the ground-state—i.e., $\Delta\mathbb{E} = \langle\Phi|\,\Lambda\overline{H}_S\,|\Phi\rangle \rightarrow \langle\Phi|\,\overline{H}_S\,|\Phi\rangle = \Delta E_{CCSD}$—their first-order time derivatives are nonzero according to the first terms in Eqs. (42) and (43). For the iterative solution of the TI-CCSD equations, I rely on the direct inversion of the iterative subspace (DIIS) method [58], which involves defining (in this case) the S

amplitudes at a given iteration as a linear combination of the amplitudes obtained at previous iterations, where the expansion coefficients are determined by minimizing the computed error. For details, I direct the reader to the literature [58].

In those cases where $\overline{H}$ is diagonalized, I employ the widely-used iterative Arnoldi method for determining the eigenvalues and eigenvectors of a non-Hermitian matrix [53], using the EOM-CC equations as the "matrix-vector" operations essential to the method. For example, in an EOM-CCSD calculation, Eqs. (60)-(62) and (65)-(67) are the matrix-vector operations needed to solve the right and left eigenvalue problems, respectively. Note that I desist from using the "two-sided" Arnoldi method, in which both the left and right eigenvalue problems are solved simultaneously, in order to avoid the convergence issues associated with it [59]. Without going into much detail, significant improvement in convergence speed can be attained by initializing the first Arnoldi vector with the $S = T$ amplitudes, which solve the TI-CCSD equations. However, I find that in several applications the two-sided Arnoldi method inevitably breaks down in this case. Thus I have instead chosen to use the one-sided Arnoldi method, whereby the left and right eigenvalue problems are addressed separately, and then impose the biorthogonality condition $\langle\tilde{\Phi}_p|\Phi_q\rangle = \delta_q^p$ at the end of the iterations. In all such computations, I adjust the number of iterations such that at minimum the low-lying excited states are converged. For the applications here, I obtain satisfactory convergence ($\delta E \leq 10^{-6}$ MeV) of the low-lying eigenvalues within an average of forty Arnoldi iterations for both the left and right eigenvalue problems.

Interacting Lipkin Systems

In 1978-79, P. Hoodbhoy and J. W. Negele provided the first documented formulation of TD-CC theory [18] and applied the method to study the dynamics of two interacting, 14-particle (fermion) Lipkin systems [19, 20]. Specifically, they computed

the excitation energy of a single system as a function of the time over which it has interacted with another system. To test my implementation of TD-CC, I repeat their calculation and compare with their results.

Explicitly, the N-particle Lipkin system comprises two, N-fold degenerate levels separated by a constant energy ϵ. As an example, Fig. 10 is representative of a 4-particle Lipkin system. As shown, the system is in its reference state, wherein all of the particles, represented by the large filled circles, occupy the lower level. Furthermore, the particles are allowed to interact via one-body and two-body forces, as depicted with the arrows in the figure. In this case, the arrows are indicative of the possibility that specific particles may be excited to states at the higher level, shown as the empty circles; however, it is understood that this is just one of many possibilities. The interactions in fact accord with the two-body Hamiltonian

$$H = \frac{\epsilon}{2}\sum_{p\sigma}\sigma a^\dagger_{p\sigma}a_{p\sigma} + \frac{V}{2}\sum_{pq\sigma}a^\dagger_{p\sigma}a^\dagger_{q\sigma}a_{q-\sigma}a_{p-\sigma} \ , \tag{72}$$

where the indices p and q are particle labels; $\sigma = \pm 1$ is indicative of the upper level and the lower level, respectively; and V is strength of the two-body interaction. From the Hamiltonian it is clear that each particle can only occupy one of two states—as shown in Fig. 10, the state in which the particle sits and the one directly above it. Hence the internal dynamics of a single Lipkin system merely involves $1p$-$1h$ and $2p$-$2h$ excitations to the higher level and $1h$-$1p$ and $2h$-$2p$ de-excitations to the lower level.

The interaction of two 4-particle Lipkin systems is illustrated in Fig. 11. From the figure, it is clear that each system has internal interactions defined by H in addition to a two-body interaction with the other system, depicted with the thick arrows and defined by the Hamiltonian

$$H_{1,2} \equiv V\sum_{p_1p_2\sigma}a^\dagger_{p_1\sigma}a^\dagger_{p_2\sigma}a_{p_2-\sigma}a_{p_1-\sigma} \ , \tag{73}$$

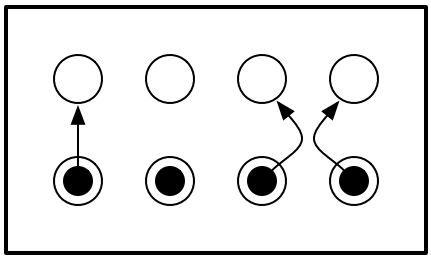

Figure 10. The 2-level, 4-particle Lipkin system.

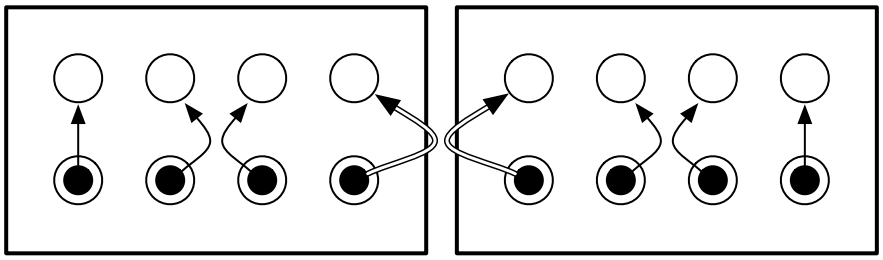

Figure 11. The interaction of two, 2-level, 4-particle Lipkin systems.

where the indices 1 and 2 are used to distinguish the two systems. Thus the total Hamiltonian of the configuration in Fig. 11 is given by the sum $H_1+H_2+H_{1,2}$. Hence, in addition to the internal dynamics of each system, $H_{1,2}$ adds the possibility of $2p$-$2h$ excitations and $2h$-$2p$ de-excitations between the two systems.

As is done in Ref. [19], I consider the case of two 14-particle Lipkin systems that are non-interacting for $t \leq 0$, such that the total Hamiltonian $H_\Sigma(t \leq 0) \equiv H_1 + H_2$, and begin to interact at $t = 0$, such that $H_\Sigma(t > 0) \equiv H_1 + H_2 + H_{1,2}$. Specifically, I observe the excitation energy,

$$\Delta E(t) \equiv \frac{1}{2}\Big(\langle\Psi| H_1 + H_2 |\Psi\rangle (t) - \langle\Psi| H_1 + H_2 |\Psi\rangle (0)\Big) , \tag{74}$$

of each system, a measure of the increase in energy that each system has undergone due to its interaction with the other system. Here the factor of $1/2$ is included since the systems are physically equivalent. (Note that $\langle\Psi| = |\Psi\rangle^\dagger$ here. See below.)

Furthermore, the initial condition is that the second term is equivalent to the ground-state CCSD energy of each (non-interacting) system.

Hoodbhoy and Negele did the computation within the Hartree-Fock basis and used the TD-CCD ($S_1 = 0$) approximation. Furthermore, to compute the expectation value $\langle\Psi|\, H_1 + H_2\, |\Psi\rangle$, they used a Hermitian approximation of the density matrices,

$$(\rho^q_p)_N = \langle\Phi|\, e^{S^\dagger}\{p^\dagger q\}e^S\, |\Phi\rangle \tag{75}$$

$$(\rho^{rs}_{pq})_N = \langle\Phi|\, e^{S^\dagger}\{p^\dagger q^\dagger sr\}e^S\, |\Phi\rangle \ , \tag{76}$$

where the subscripts N and curly brackets $\{\ldots\}$ are indicative of the normal ordered forms. Though these "approximate" densities are easily expanded in terms of the S amplitudes and their products, they are non-terminating due to the exponential nature of the excitation operators and thus must be truncated at some level. Note that this is in stark contrast to the exact densities of the bi-variational formalism [see Eqs. (50) and (51)], which have finite expansions due to the linearity of Λ; however, in 1978, the bi-variational formulation of TD-CC had not yet materialized. Thus Hoodbhoy and Negele instead assumed $\langle\Psi| = \langle\Phi|\, e^{S^\dagger}$ to be the parameterization of the left wavefunction. Note that this assumption is in fact *correct*: in the limit that the exponentials in Eqs. (75) and (76) are expanded indefinitely, the exact densities are recovered since, in that case, $\langle\Phi|\, e^{S^\dagger}$ is the exact left wavefunction due to the fact that the operator $e^{S^\dagger}$ induces all possible de-excitations. (It straightforward to show that the operator $S^\dagger$ is, like Λ, linear in de-excitations.)

Within a trial computation, I determined that contributions to the approximate densities which are higher in order than those quadratic in the s^{ab}_{ij} amplitudes are negligible in the computation of the observable in *this* problem [see Eq. (74)]: thus I choose to truncate the densities at the quadratic terms for computational efficiency. Note that I have found this approximation to be insufficient for computing the correct binding energy [see Eq. (46)] of ^{4}He and furthermore speculate that one may need to

include within the approximate densities terms up to fourth-order in s_{ij}^{ab} in order to obtain the correct binding energy. At this order, the densities would together comprise more than 200 diagrams. Furthermore, truncation at the quadratic terms still involves an extensive number of contributions (≈ 60 diagrams). Thus the theoretical appeal of the approximation made in Eqs. (75) and (76) is in check when considering that the densities in Eqs. (50) and (51) are exact and together comprise ≈ 45 diagrams. For this reason and, furthermore, since the approximate densities are unimportant for other applications, I refrain from providing their diagrammatic and algebraic expansions and instead direct the interested reader to Ref. [4].

For the computation of the excitation energy [see Eq. (74)], I set $\epsilon = 1$ and choose $NV = 5$ such that $V = 0.357$ is well into the strong-coupling region of the Lipkin system. Note that Hoodbhoy and Negele did this to ensure that they would obtain a non-trivial time-dependent Hartree-Fock (TDHF) result [60] for comparison with the TD-CCD result [19]. I solve the TI-CCD equation [see Eq. (56)] in order to put each system in its ground state at $t = 0$ and thereby obtain $\langle\Psi|\, H_1 + H_2\,|\Psi\rangle\,(0)$; add the interacting term $H_{1,2}$ to the Hamiltonian; and time-evolve the s_{ij}^{ab} amplitudes [see Eq. (31)] for 12×10^{-23} s, making 90 time steps of size 0.4 fm/c, while periodically computing the excitation energy. Specifically, using the approximate densities [see Eqs. (75) and (76)], I compute the one-body and two-body parts of the expectation value $\langle\Psi|\, H_1 + H_2\,|\Psi\rangle$ as is done in Eqs. (53) and (54). The result obtained for the excitation energy and that obtained by Hoodbhoy and Negele are shown in Fig. 12. The results are clearly identical. Note that the exact and TDHF results, both taken from Ref. [19], are also shown for the purpose of illustrating the increased accuracy of TD-CCD relative to TDHF. The difference in accuracy between the two methods is expected since TD-CCD allots for higher-order many-body correlations than TDHF. In fact, it is straightforward to show that TDHF is equivalent to TD-CCS in the HF basis. Recall from the discussion at the beginning of the previous chapter that

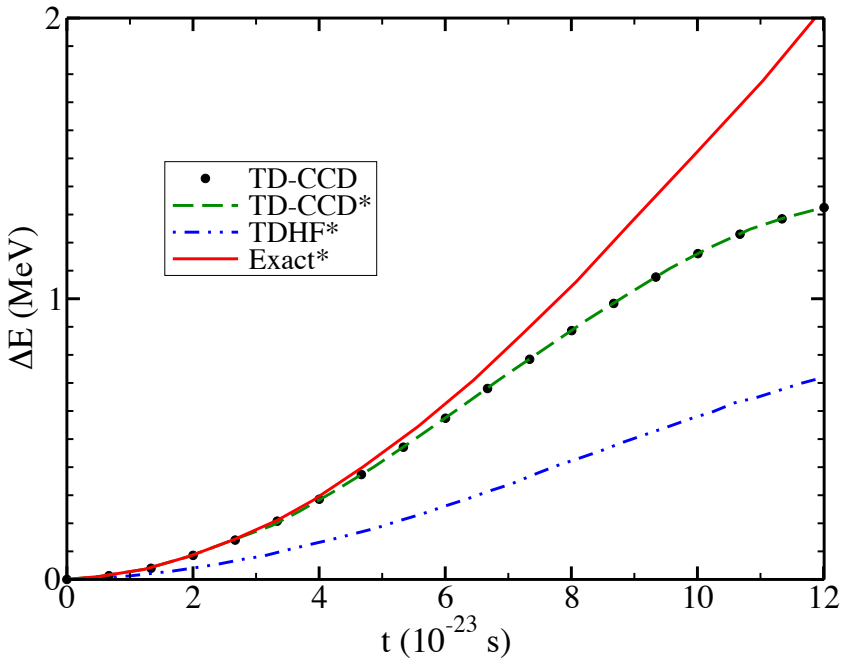

Figure 12. TD-CCD result for the excitation energy as a function of time for two interacting, 2-level, 14-particle Lipkin systems. Hoodbhoy and Negele's results for the TD-CCD, TDHF, and exact computations are noted with an asterisk and were taken from Ref. [19].

$\langle \Phi_i^a | \, \overline{H} \, | \Phi_{HF} \rangle = 0$; thus $S_1 = 0$ in the HF basis. So if we rewrite the TD-CCS equation [see Eq. (30)] as

$$i\hbar \, \langle \Phi | \, a_i^\dagger a_a e^{-S} \partial_t e^S \, | \Phi \rangle \;\; = \;\; \langle \Phi | \, a_i^\dagger a_a \overline{H} \, | \Phi \rangle \tag{77}$$

and consider the equation in the HF basis, we obtain that

$$\langle \Phi | \, a_i^\dagger a_a \big(i\hbar \partial_t - H \big) \, | \Phi \rangle = 0 \; , \tag{78}$$

which is precisely equivalent to the TDHF equation [9]. Since the CCS (CCD) approximation accounts for up to—but not all—effective two-body (six-body) correlations, as I discuss in more detail later, the discrepancy between TD-CCD and TDHF in Fig. 12 is indeed expected. In fact, I attribute the discrepancy between the TD-CCD and exact results to the neglect of higher-body correlations. This, of course, could be determined if one were to do a TD-CCSDT computation of the excitation energy.

The result shown in Fig. 12 implies that at the least my implementation of the solutions of the TI-CCD and TD-CCD equations are most-probably correct. Furthermore, in a separate calculation, I have confirmed my suspicion that the result obtained here, which again incorporates all of the non-negligible terms of the approximate density matrices, is identical to that obtained within the bi-variational approach, whereby energy is computed exactly (relative to the chosen approximation) according to Eq. (46). Specifically, I have done the calculation using bi-variational TD-CCD and found the result to be equivalent and identical to the TD-CCD result shown in Fig. 12. All of this considered, I conclude that my implementation of bi-variational TD-CC is correct. While it may be argued that this supposition is dependent upon the accuracy of Hoodbhoy and Negele's result, it is somewhat improbable that the computations discussed here would all replicate the same inaccuracy.

Single Lipkin System

For a simple test of the exact density—here, only the one-body part [see Eq. (50)]—I apply bi-variational TD-CCSD [see Eqs. (37) and (41)] to time-evolve the expectation value of the one-body operator

$$J_z \;=\; \frac{1}{2}\sum_{p\sigma}\sigma a^{\dagger}_{p\sigma}a_{p\sigma} \tag{79}$$

for a single, 2-level, 14-particle Lipkin system. It is clear from the Lipkin Hamiltonian [see Eq. (72)] that J_z is, apart from the factor ϵ, equivalent to the one-body interaction. I use the parameters $\epsilon = 1$ and $V = 0.04$ such that the system lies in the weak-coupling region, well-within the boundary of the phase transition which occurs at $(N-1)V = \epsilon$ [19], and furthermore the initial conditions $S = 0 = L$ and a time-step width of 0.5 fm/c for 6000 iterations. To compute the expectation value $\langle J_z\rangle$, I employ the exact one-body density [see Eq. (50)] and Eq. (53). Fig. 13 demonstrates

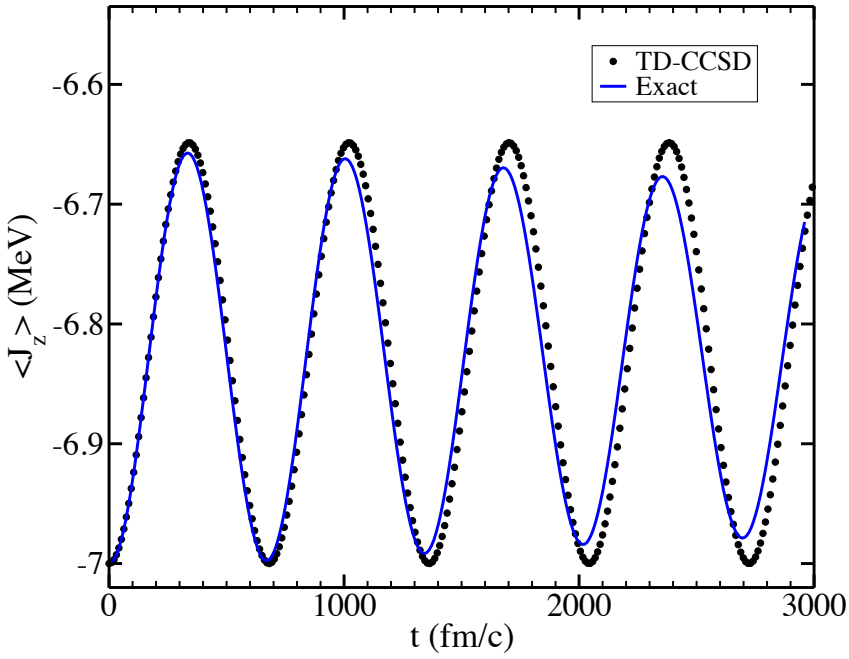

Figure 13. Bi-variational TD-CCSD evolution of J_z for a 2-level, 14-particle Lipkin system with $V = 0.04$. The exact result is also shown. For the TD-CCSD result, one of twenty-one computed points is shown.

that the result is in reasonable agreement with the exact result. Note that for larger values of V the result is expected to deviate more from the exact solution due to the deformation of the energy surface which occurs at the phase transition [61]. To illustrate this, I solve the problem using $V = 0.08$, which is just at the phase transition, and provide the result in Fig. 14. Note that doing the computation in the HF basis does not improve the result significantly enough for consideration; thus, in order to improve the accuracy appreciably, I speculate that it may be necessary to use multi-reference coupled-cluster methods, which are often used to study systems at or near a phase transition [4]. Since I have not yet applied such methods, I will not deliberate them here.

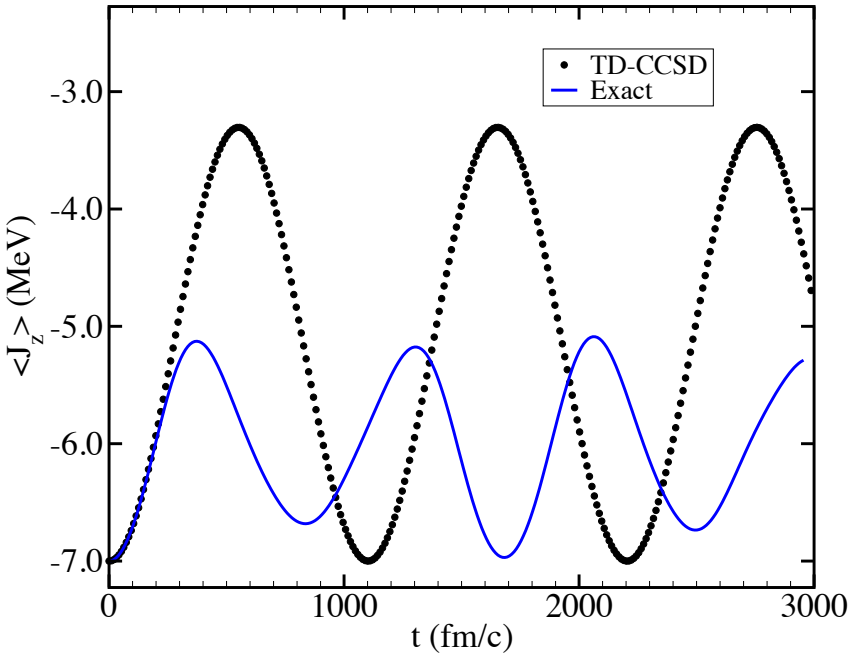

Figure 14. Bi-variational TD-CCSD evolution of J_z for a 2-level, 14-particle Lipkin system with $V = 0.08$. The exact result is also shown. For the TD-CCSD result, one of twenty-one computed points is shown.

Nuclear Excited States

Though the traditional approach to obtaining the excited states and associated excitation energies of a nucleus within the coupled-cluster formalism is to solve the equations of motion [see Eqs. (63) and (68) for the left and right eigenvalue problems of $\overline{H}$], an alternative approach exists within the time-dependent formalism. To see this, consider the exponential nature of the parameterization of the right wavefunction [see Eq. (9)] and that, at any moment in time, the wavefunction may also be written as [62]

$$|\Psi\rangle \;=\; \sum_q c_q(t)\,|\Psi_q\rangle \;=\; \sum_q c_q(0) e^{-\frac{i}{\hbar}E_q t}\,|\Psi_q\rangle \;\;, \tag{80}$$

where $|\Psi_q\rangle$ is the q-th eigenstate of H; E_q is the corresponding energy; and $c_q(t)$ is the corresponding expansion coefficient, which is time-dependent in this case. Thus

if we consider the Fourier transform of the auto-correlation function,

$$\langle \Psi(0)|\Psi(t)\rangle \;=\; \sum_q |c_q|^2 e^{-\frac{i}{\hbar}E_q t} \;, \tag{81}$$

we obtain straightaway that

$$F(\omega) \;=\; \sum_q |c_q|^2 \int e^{-\frac{i2\pi}{\hbar}(E_q-\hbar\omega)} dt \;=\; \hbar \sum_q |c_q|^2 \delta(E_q - \hbar\omega) \;, \tag{82}$$

which clearly has peaks at frequencies conjugate to excited-state energies [50]. Furthermore, since any excitation amplitude $s^{a_1\ldots a_n}_{i_1\ldots i_n}$ can be related to $\langle \Phi^{a_1\ldots a_n}_{i_1\ldots i_n}(0)|\Phi^{a_1\ldots a_n}_{i_1\ldots i_n}(t)\rangle$, it is deduced that the Fourier transform of any excitation amplitude should provide a spectrum of excited-state energies. Note that the deduction made here is consistent with a much more-rigorous derivation of the same result, given in Ref. [63] in the context of coupled-cluster linear response methods. From this, it is clear that a different way to obtain the spectrum of excited-state energies for a given nucleus is to time-evolve the S amplitudes [see Eq. (37)] and subsequently compute the Fourier transform of *any* S amplitude.

I apply this method to determine the excited-state energies of the nuclei ^{4}He and ^{16}O. In both cases, I solve the TI-CCSD equations [see Eqs. (55) and (56)], perturb each of the $S = T$ amplitudes by a small random number of order 10^{-3} at $t = 0$, and then time-evolve the amplitudes [see Eqs. (30) and (31)] while recording the evolution of a single, randomly-selected amplitude. (Note that it is unnecessary to time-evolve the Λ amplitudes since this analysis depends on S only. Further note that a more smooth Fourier spectrum may be obtained by instead time-evolving many randomly-selected amplitudes and then averaging the corresponding Fourier transforms.) For computational efficiency, I employ a time-step width of 1 fm/c and run to 20000 fm/c for ^{4}He and 6000 fm/c for ^{16}O. I then compute a Fourier transform of the amplitude selected in each case. The resulting spectra for ^{4}He and ^{16}O are shown in Figs. 15 and 16, respectively. In each plot, energies are measured relative to the ground-state,

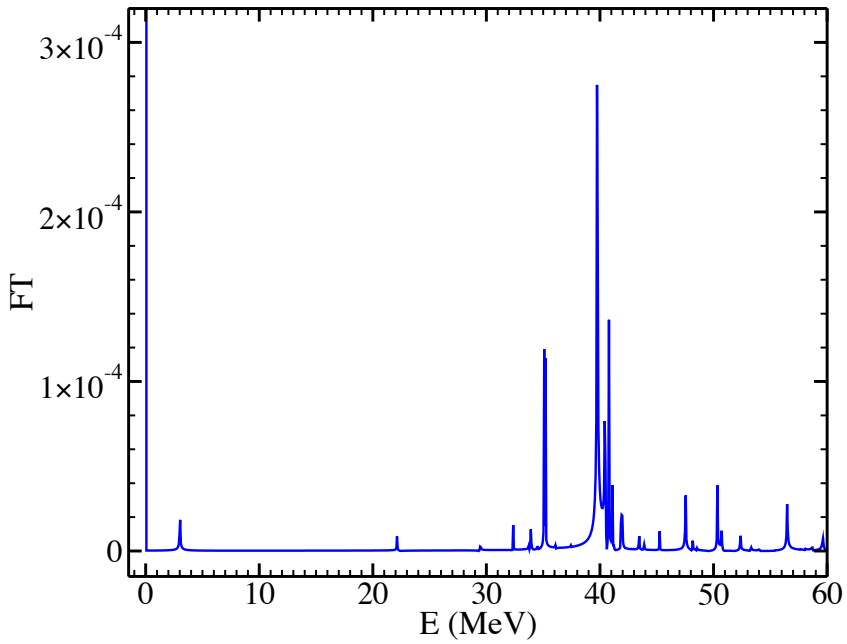

Figure 15. Fourier transform of a randomly-selected S amplitude for the ^{4}He nucleus.

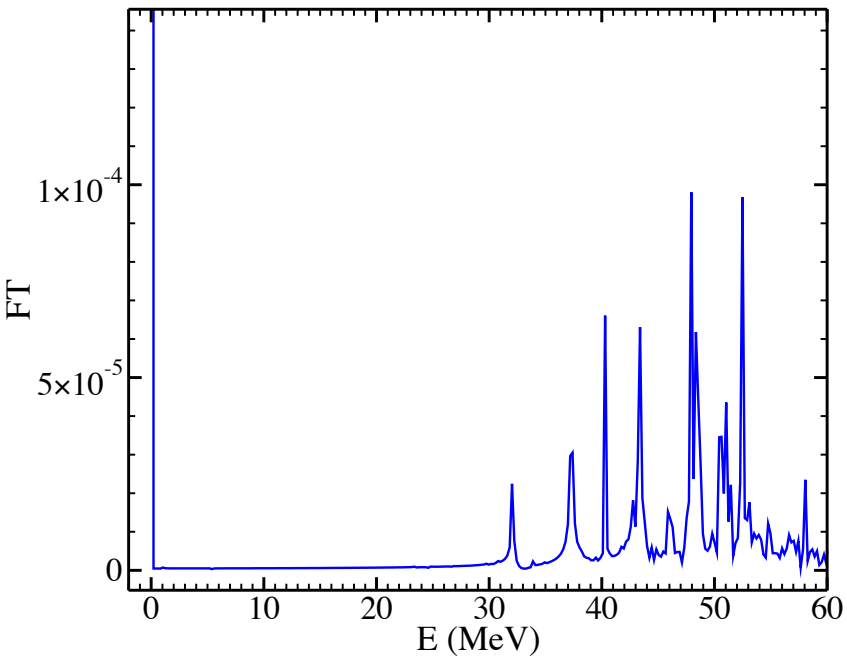

Figure 16. Fourier transform of a randomly-selected S amplitude for the ^{16}O nucleus.

which corresponds to the peak at $E = 0$. This is natural since the time evolution of the S amplitudes depends only on the normal-ordered elements of $\overline{H}$—i.e., the elements of $\overline{H}_S \equiv e^{-S} H_N e^S$. Furthermore, the energies have uncertainties—$\delta E = 2\pi\hbar c/T$, where T is the total time of the evolution, measured in fm/c—of $\delta E \approx 0.06$ MeV for ^{4}He and $\delta E \approx 0.2$ MeV for ^{16}O. (Thus the accuracy of the computation could be improved by evolving to larger T.)

To confirm the validity of this computation, from each plot, I select four peaks at random and compare the associated energies with those obtained separately by solving the EOM-CCSD equations [see Eqs. (60)-(62)] directly. The comparisons for ^{4}He and ^{16}O are recorded in Tables 1 and 2, respectively. Note that all of the peaks shown in Figs. 15 and 16 are associated with values obtained by solving the EOM-CCSD equations; only four values are compared here since the number of results is quite numerous. Furthermore, the agreement between all values is reasonable, and in every case the difference lies within the associated energy uncertainty.

Clearly the energies corresponding to the peaks in Figs. 15 and 16 are not all associated with real, physical states and are furthermore under-bound [2]. Through a series of trial computations, I have confirmed that the under-binding arises merely from the limitation to an unrealistically-small model space; thus the effect can be reduced by using a larger model space. For example, if the size of the model space is increased by merely one shell (to a total of five shells)—i.e., up to the third s-1/2 level—all of the peaks in Fig. 15 are shifted to the left. For instance, the giant peak at ≈ 40 MeV is shifted to ≈ 32 MeV; the small peak at ≈ 3 MeV is shifted to ≈ 2.4 MeV (probably the 0^+ state [2]). Though these are substantial differences, they are not nearly enough for comparison with experimental data. In fact, benchmark calculations employing a similar low-momentum, two-body Hamiltonian have shown that the CCSD energy [see Eq. (57)] for ^{4}He is not even well-converged at model-space sizes ≤ 12 shells [41]. Furthermore, it is understood that the accuracy of results may

Table 1. Comparison of selected excited-state energies obtained using TD-CCSD and EOM-CCSD for ^{4}He. Energies are given in units of MeV. The uncertainty in the TD-CCSD energies is $\delta E \approx 0.06$ MeV.

	TD-CCSD	EOM-CCSD
E_1	3.04	3.02
E_2	29.45	29.47
E_3	35.52	35.53
E_4	41.10	41.11

Table 2. Comparison of selected excited-state energies obtained using TD-CCSD and EOM-CCSD for ^{16}O. Energies are given in units of MeV. The uncertainty in the TD-CCSD energies is $\delta E \approx 0.2$ MeV.

	TD-CCSD	EOM-CCSD
E_1	32.20	32.29
E_2	33.85	33.91
E_3	37.40	37.60
E_4	48.15	48.12

be improved by the inclusion of three-nucleon forces [48], more-nucleon forces, and/or less-restrictive truncations of the cluster operators.

The presence of unphysical states in the spectra is due to the incomplete separation of the center-of-mass motion. In Ref. [64], the authors have shown that thecoupled-cluster wavefunction can be only approximately factorized into intrinsic and center-of-mass parts—i.e., $\Psi \approx \Psi_{int}\Psi_{com}$—and that, as expected, the number of spurious states that will be resolved in these computations increases (decreases) with a decrease (increase) in the degree of factorization. Furthermore, a higher degree of factorization is observed within larger model spaces; therefore, since the model space used in this work is unreasonably-small, it is not surprising that the results here include spurious states.

Energy

Since the introduction and initial application of TD-CC theory [18, 19], its usage within the scientific community has been quite infrequent. This is no doubt due to the confusion that inevitably arose while attempting to consider the concept of energy in TD-CC prior to Kvaal's recent bi-variational formulation of the method [31]. For example, the authors of Ref. [29] noted that the element $\overline{H}_0 \equiv \langle\Phi|\,\overline{H}_S\,|\Phi\rangle$, which is the ground-state correlation energy when the TI-CC equations [see Eqs. (55) and (56) for the CCSD approximation] are satisfied, incurs large-amplitude oscillations—up to several MeV within the applications that I have done—if the S amplitudes are time-evolved and furthermore attains an imaginary component. To confirm the noted instability in $\overline{H}_0$, I compute the element as a function of time for the deuteron (the ^{2}H nucleus) and show a plot of its real part, labeled "$\overline{H}_0$" in Fig. 17. In this case, the variation in $\overline{H}_0$ is larger in magnitude than even the CCSD ground-state binding energy "E_0," also shown in the figure (but explained later). Furthermore, during the evolution, $\overline{H}_0$ quickly develops an imaginary part which oscillates within a maximum magnitude ≈ 2.5 MeV. From these results, it is clear that $\overline{H}_0$ can not be an energy: in the time-dependent formalism, it is merely an element of the similarity-transformed Hamiltonian $\overline{H}$. One can further conjecture that energy and other observables may be computed by time-evolving the eigenvalue problem of $\overline{H}$—i.e., integrating the S amplitudes [see Eq. (37)] while periodically computing the eigenvalues and eigenvectors of $\overline{H}$ using the EOM-CC equations [see Eq. (63)]. However, as I will show, the shortfall of this method is that for computational viability one must truncate the Hilbert space in which the diagonalization of $\overline{H}$ is done. The truncation in turn renders the diagonalization inexact; consequently, the computed energies are not fully-conserved. Fortunately, it is now known that the functional $\mathbb{E}$ [see Eq. (18)] is the appropriate TD-CC energy functional; it is manifestly-conserved by definition [see Eq. (44)].

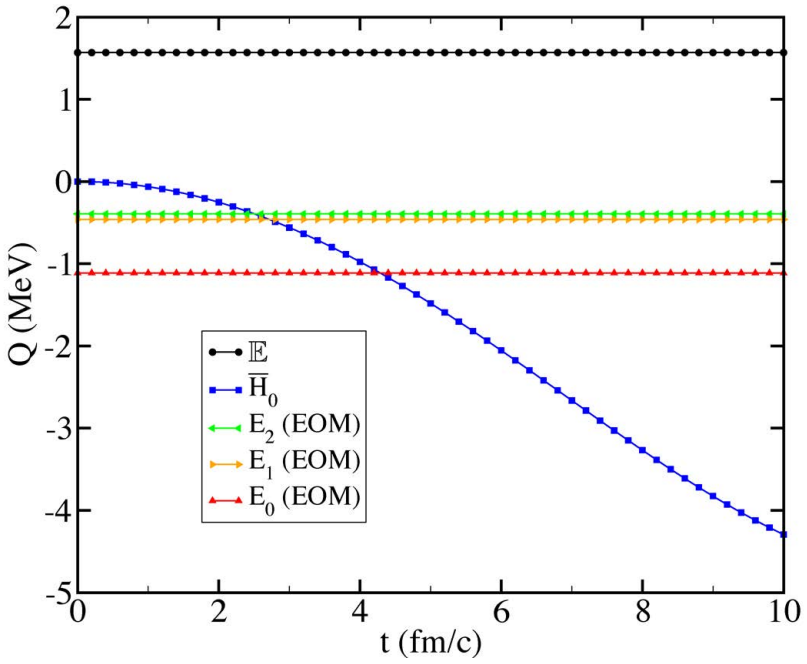

Figure 17. Some time-evolved quantities Q for the ^{2}H nucleus: the coupled-cluster energy functional $\mathbb{E}$; the element $\overline{H}_0$; and the lowest three eigenvalues E_0, E_1, and E_2 of $\overline{H}$. In all cases, one of two computed points is shown.

In this section, I examine the energy of nuclei using the latter two approaches. Specifically, I consider the real-time evolutions of both the functional $\mathbb{E}$ and the eigenvalues of $\overline{H}$, demonstrating the conservation of the former and the inexactness of the latter when the Hilbert space is truncated. I then show that the imaginary-time evolution of the eigenvalues of $\overline{H}$ is in fact useful within the suppression of excitations and thus the recovery of the ground state wavefunction, a computation which is not possible in the bi-variational formalism since the associated functional $\mathbb{E}$ is complex-analytic in time.

Real-time evolution of $\mathbb{E}$

I demonstrate the conservation of $\mathbb{E}$ first by computing its value as a function of time for the deuteron. Using the initial conditions $S = 0 = \Lambda$, and thereby initializing the energy to the Fermi vacuum expectation value of H [see Eq. (23)], I time-evolve the S and Λ amplitudes [see Eqs. (30), (31), (39), and (40)], using a time-step width

of 0.1 fm/c, and periodically compute the total binding energy $\mathbb{E}$. Fig. 17 shows the result, labeled "$\mathbb{E}$." Note that the energy is positive because the coupled-cluster correlations are suppressed by the initial conditions. For a more stringent test of conservation, I compute $\Delta\mathbb{E}(t) \equiv \mathbb{E}(t) - \mathbb{E}(0)$ for the ^{4}He nucleus, using the same initial conditions ($S = 0 = \Lambda$) but instead using a time-step width of 0.05 fm/c. The result is shown in Fig. 18. Note that the energy remains within $\approx 10^{-9}$ MeV of the Fermi vacuum expectation value of H throughout the evolution. Though the functional $\mathbb{E}$ is, in theory, exactly-conserved due to the fact that it is stationary and complex-analytic, in practice it varies by a small amount, which I find to have a remarkable dependence on the time-step width used. For example, in the application to ^{4}He, if I instead use a time-step width of 1 fm/c, I observe changes in energy of order $\approx 10^{-2}$ MeV. Upon further inspection, I find that this is due primarily to rapid (yet continuous) changes in the Λ amplitudes as a function of time. As expected, this renders the precision of the RK4 approximation highly-dependent on the step size used. (Note that the S amplitudes do not vary so rapidly. Recall that I used a time step width of 1 fm/c to obtain the nice results in Figs. 15 and 16.)

Real-time evolution of $\overline{H}$

One can attempt to compute energy instead by time-evolving the eigenvalue problem of the similarity-transformed Hamiltonian $\overline{H}$. Specifically, the computation involves an interplay between the solution of the TD-CC, S equations [see Eq. (37)] and the periodic diagonalization of $\overline{H}$ using the EOM-CC equations [see Eq. (63) or (68)]. Recall that the Λ amplitudes are not needed to solve the EOM-CC equations.

I perform the computation for the deuteron as an initial example. After solving the TI-CCSD equations [see Eqs. (55) and (56)] and then perturbing the resulting S amplitudes, I time-evolve the amplitudes according to the TD-CCSD equations [see Eqs. (30) and (31)], using a time-step width of 0.1 fm/c, and at each iteration diagonalize $\overline{H}$ by solving its right eigenvalue problem [see Eqs. (60)-(62)]. During

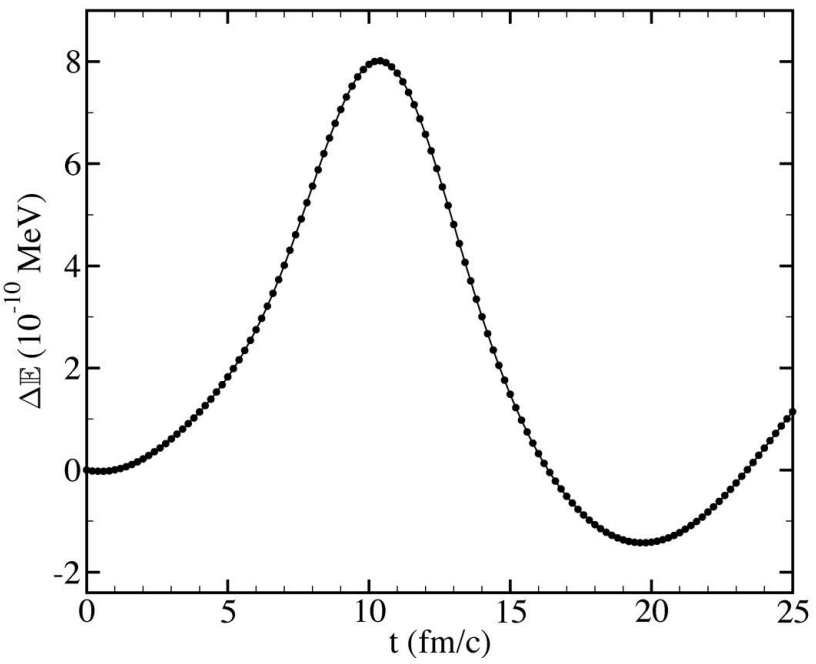

Figure 18. $\Delta\mathbb{E}(t) \equiv \mathbb{E}(t) - \mathbb{E}(0)$ for the ^{4}He nucleus. One of four computed points is shown.

the evolution, the lowest three eigenvalues of $\overline{H}$ are converged to within 10^{-6} MeV and recorded. The results are shown in Fig. 17 and are denoted $\{E_0, E_1, E_2\}$. Note that the value of $E_0 \approx -1.11$ MeV is very close to but slightly less-bound than the ground-state energy $E_{CCSD} \approx -1.12$ MeV in the model space used. This is expected since, at $t = 0$, the S amplitudes are perturbed slightly away from the values which solve the TI-CCSD equations; thus the system is placed in a state less-bound than its true ground-state. The most important thing to note here is that the eigenvalues of $\overline{H}$ are, for practical purposes, conserved. This is as expected: the e^S-mediated similarity transformation of a time-independent Hamiltonian H should have stationary eigenvalues.

Nonetheless, this is only true provided that *both* the similarity transformation of H *and* the diagonalization of the resulting $\overline{H}$ are carried out exactly. Note that by *exact* diagonalization I am referring merely to the convergence of the eigenvalues

of interest (to within the desired precision—$\delta E \leq 10^{-6}$MeV for these computations) within a basis which is un-truncated relative to the number of nucleons—and not actually to the *full* diagonalization of $\overline{H}$. Recall that in the CCSD approximation the Baker-Campbell-Hausdorff expansion [see Eq. (25)] yields up to six-body terms in $\overline{H}$ [49] and that solving the EOM-CCSD equations is equivalent to diagonalizing $\overline{H}$ in a Hilbert space which includes up to $2p$-$2h$ excited states. I add here that the EOM-CCSD equations account for up to only a few of the three-body terms of $\overline{H}$ [see Figs. 35-37 and the associated Eqs. (117)-(119)]. Thus it is clear that the computation discussed above for the deuteron is exact on both accounts: neither the similarity-transformation of H nor the basis is truncated relative to the number of nucleons. For larger systems, however, it is generally necessary to truncate the basis—and thereby $\overline{H}$—in order to render the computation viable. Such truncations in turn render the similarity-transformation inexact and the eigenvalues of $\overline{H}$ non-conserved.

To show this, I consider three distinct cases for both the ^{3}H nucleus (the triton) and the ^{4}He nucleus. All cases use the initial condition $S = 0$; thus $E(0)$ is equivalent to the Fermi vacuum expectation value of H [Eq. (23)].

In Case (i), I do exactly what I have done for the deuteron but consider only the lowest eigenvalue E_0 of $\overline{H}$: perform a TD-CCSD evolution of the S amplitudes and periodically diagonalize $\overline{H}$ in a basis including up to $2p$-$2h$ excited states. While this method introduced no truncations for the deuteron ($A = 2$), it clearly has truncations both in $\overline{H}$ and the basis for a system with $A > 2$. Note the instability in the results of Case (i), labeled "TD-CCSD ($2p$-$2h$)" in Figs. 19 and 20 for the triton and ^{4}He, respectively. As expected, the average amplitude of the oscillations in E_0 are smaller for the triton since both truncations are albeit closer to its reality.

In Case (ii), I instead employ a TD-CCS ($S_2 = 0$) evolution [see Eq. (30)] while retaining the basis size at the $2p$-$2h$ level. Since in the CCS approximation the expansion of $\overline{H}$ includes up to only two-body terms [see Fig. 31], in Case (ii) there

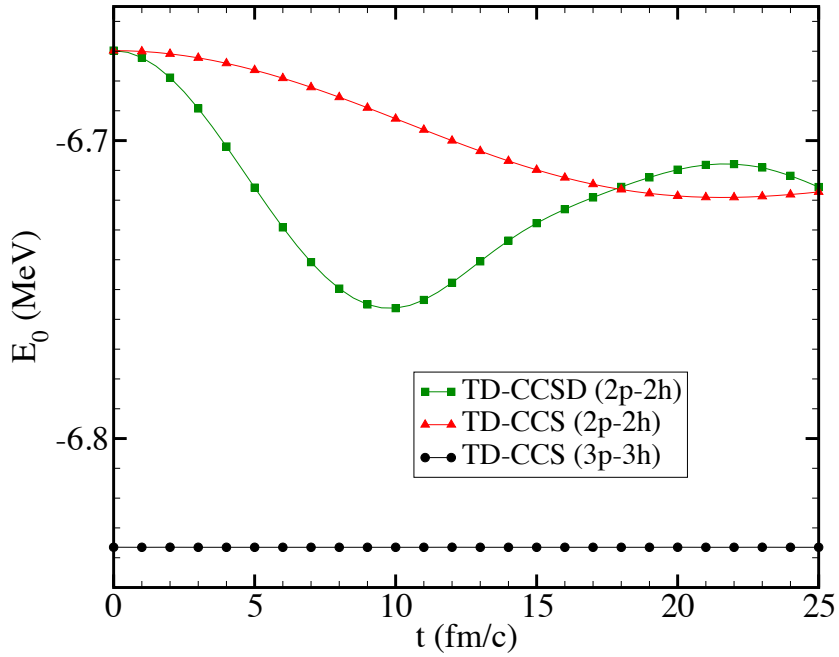

Figure 19. The lowest eigenvalue E_0 of $\overline{H}$ for the ^{3}H nucleus, computed in the three ways discussed in the text.

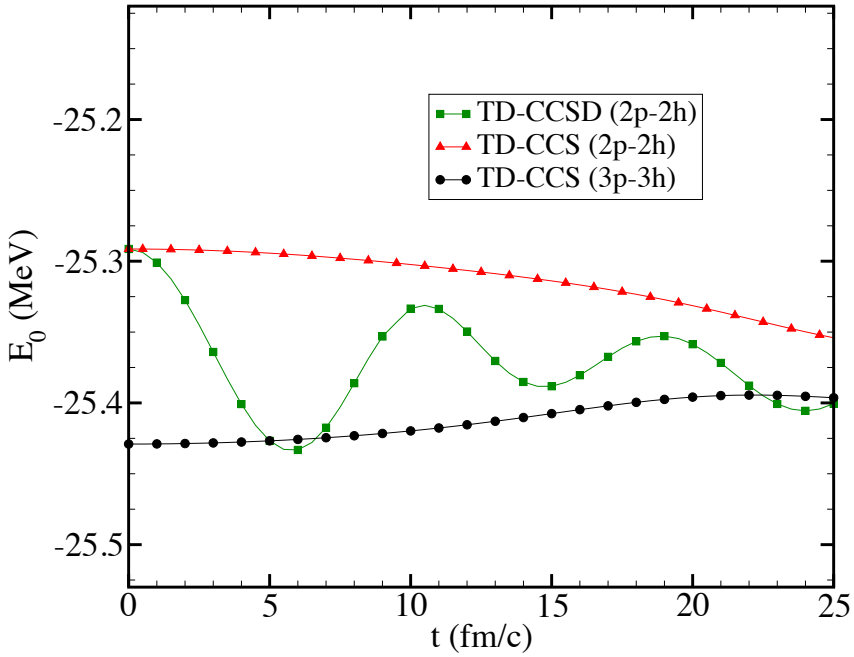

Figure 20. The lowest eigenvalue E_0 of $\overline{H}$ for the ^{4}He nucleus, computed in the three ways discussed in the text.

are no truncations to $\overline{H}$ for either system. The results of Case (*ii*) are labeled "TD-CCS (2*p*-2*h*)" in Figs. 19 and 20. Note that the average amplitudes and frequencies of the oscillations are, as expected, less than in Case (*i*); they nonetheless remain significant. Furthermore, note that the average amplitudes of the oscillations are smaller for the triton—again, since the truncation to the 2*p*-2*h* basis is less severe for the three-nucleon system.

In Case (*iii*), I again perform a TD-CCS evolution but instead periodically diagonalize $\overline{H}$ in a basis including up to 3*p*-3*h* excited states. Note that such diagonalization involves the solution of the EOM-CCSDT equations [see Appendix F]. In this approximation, *no* truncations are made to either $\overline{H}$ or the basis for the triton; however, the basis remains truncated relative to the ^{4}He nucleus. The results, labeled "TD-CCS (3*p*-3*h*)" in Figs. 19 and 20, are thus as expected: E_0 is completely conserved only for the triton. Note that $E_0(0)$ is less in Case (*iii*) than in Cases (*i*) and (*ii*) since a larger number of binding correlations are incorporated with the larger basis.

These results clarify that in practical applications the real-time evolution of the eigenvalue problem of $\overline{H}$ is unwarranted for the computation of the spectrum—thus observables. For nuclei larger than $A = 2$, it is almost essential to truncate $\overline{H}$, the basis, or in most cases both. Note, however, in contradiction to what may be expected, truncations to both $\overline{H}$ and the basis do not have a significantly-greater effect for larger systems. To show this, I perform the Case (*i*) computation for the ^{16}O nucleus and show the result in Fig. 21. It is clear from the figure that the average fluctuation in E_0 is less than one percent of the CCSD binding energy $E_{CCSD} \approx 145$ MeV in this case. Taking this into consideration, it seems that the approximation is not worse—but in fact somewhat better—for larger systems since they are naturally more well-bound.

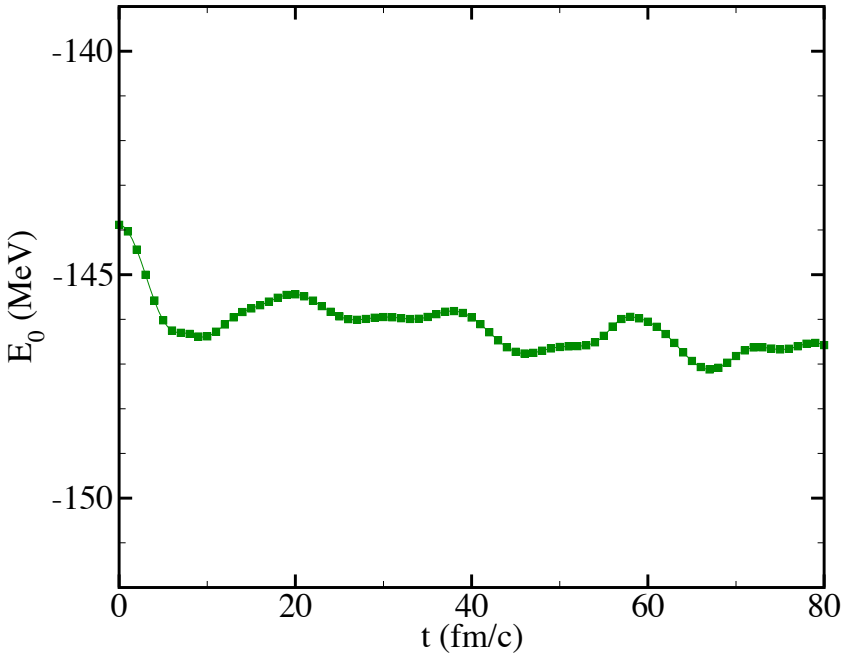

Figure 21. The lowest eigenvalue E_0 of $\overline{H}$ for the ^{16}O nucleus, computed using TD-CCSD in a $2p$-$2h$ basis.

Imaginary-time evolution of $\overline{H}$

It is well-known that the imaginary-time propagation of a wavefunction serves to suppress excitations and to thereby project out the ground-state. To see this, consider the propagator terms $e^{-iE_q t}$ in the expansion of Eq. (80). From these terms it is clear that if $\tau \equiv it$, as τ grows, the excited-state contributions to the wavefunction are suppressed; and the total energy is thereby reduced. Furthermore, since the general solution to the time-dependent Schrödinger equation can be written alternatively in terms of the total energy E as [62]

$$|\Psi(t)\rangle \;=\; e^{-iEt}\,|\Psi(0)\rangle \;, \tag{83}$$

it is clear that the reduction in energy $\langle\Psi(\tau)|\,H\,|\Psi(\tau)\rangle$ must be proportional to a factor $e^{-(E-E_q)\tau}$; thus at large τ, when E becomes equivalent to E_0—the lowest, ground-state energy—the τ-evolution no longer has an affect on the wavefunction.

At this point, the suppression of excitations is complete, and only the ground-state remains in the expansion of $|\Psi(\tau)\rangle$.

Note that imaginary-time "projection" is *not* possible in the bi-variational TD-CC formalism. Due to the fact that the functional $\mathbb{E}$ is complex-analytic in time, its value can not decay exponentially. In his recent article [31], Kvaal discusses this in some detail. However, as is shown in the previous subsection, the explicit propagation of the eigenvalues of $\overline{H}$ is inexact and thus non-conservative. Consequently, the imaginary-time suppression of excitations is possible in that formalism.

Here I provide an example for the ^{4}He nucleus. Substituting $\tau \equiv it$ in the TD-CCSD, S equations, we obtain

$$\partial_\tau s_i^a = -\langle \Phi_i^a | \, e^{-S} H e^S \, | \Phi \rangle \tag{84}$$

$$\partial_\tau s_{ij}^{ab} = -\left\langle \Phi_{ij}^{ab} \right| e^{-S} H e^S \, | \Phi \rangle \tag{85}$$

as the appropriate evolution equations. Using the initial condition $S = 0$—which, as discussed in previous applications, initializes the energy to the Fermi vacuum expectation value of H [Eq. (23)] and thereby excludes the effect of the energy-reducing coupled-cluster correlations—I propagate the S amplitudes according to Eqs. (84) and (85) while periodically computing the lowest eigenvalue E_0 of $\overline{H}$. Throughout the evolution, $\Delta E_0(\tau) \equiv |E_0(\tau) - E_{CCSD}|$ is recorded, where E_{CCSD} is the CCSD ground-state energy [see Eq. (57)], computed after solving the TI-CCSD equations [see Eqs. (55) and (56)]. I use 400 time steps of width 0.5 fm/c. The result is plotted in Fig. 22, from which it is clear that the convergence to the ground-state is indeed exponential. Note that the instability that develops in the plot at $\tau \approx 175$ fm/c is due to the fact that ΔE_0 is in close proximity to my convergence criterion for E_0, $\delta E_0 \leq 10^{-6}$ MeV.

It is also instructive to visualize the τ-evolution of $\overline{H}$. For this purpose, I refer back to the 3x3 block form of $\overline{H}$ [see Eq. (36)]. During the evolution discussed above,

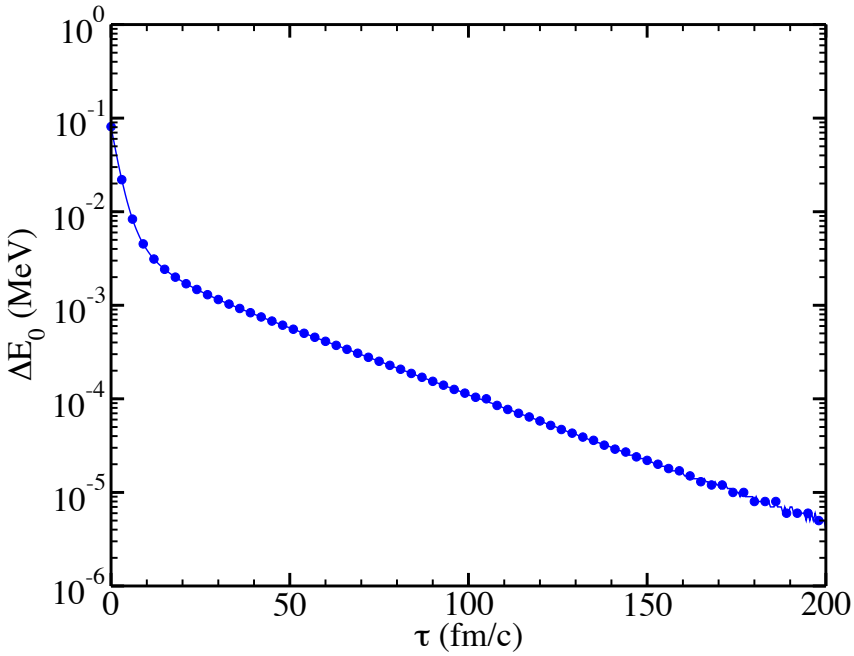

Figure 22. $\Delta E_0(\tau) \equiv |E_0(\tau) - E_{CCSD}|$ for the ^{4}He nucleus, where $\tau \equiv it$.

I record as a function of τ the logarithms of the averages of the magnitudes of all of the elements within a given block of $\overline{H}$. Fig. 23 shows contour plots of the results taken at $\tau = 0$ fm/c and $\tau = 200$ fm/c, respectively. Note that at $\tau = 0$, $\overline{H} = H$, which is Hermitian and thus symmetric. Then, as τ grows, coupled-cluster correlations are added and $\overline{H} \neq H$ is non-symmetric. By the end of the evolution, the elements $\overline{H}_i^a$ and $\overline{H}_{ij}^{ab}$ have become negligible, which is indicative that the TI-CCSD equations have been satisfied and therefore the total energy is equivalent to the ground-state CCSD value.

In Ref. [36], it is suggested that the τ-evolution of $\overline{H}$, given by

$$\partial_\tau \overline{H}(\tau) \quad = \quad [\partial_\tau S, \overline{H}(\tau)] \tag{86}$$

—i.e., the τ-generalization of the identity $\dot{\overline{H}} = [\overline{H}, \dot{S}]$, which was used to arrive at the result in Eq. (44)—is somewhat similar to the similarity-renormilization-group (SRG) equations often used in the taming of interactions [54, 65–68] and more-recently in

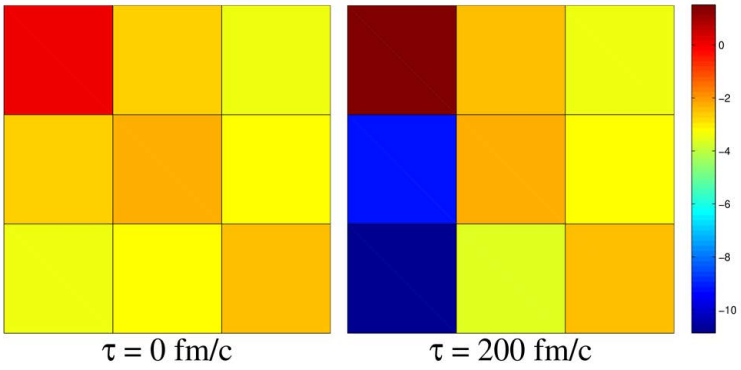

Figure 23. Logarithmic averages over the elements of $\overline{H}$ for the ^{4}He nucleus at $\tau = 0$ fm/c and $\tau = 200$ fm/c, where $\overline{H}$ has the form given in Eq. (36).

nuclear structure computations [69]. Further examination of the connection between these two methods is an avenue for future research.

CHAPTER IV

CONCLUSIONS

I have demonstrated that the bi-variational formulation of time-dependent coupled-cluster theory is suitable for the study of intrinsic nuclear properties. Within applications to Lipkin systems, I have found that results compare nicely with exact results, indicating that my implementation of the method is correct. Furthermore, in proof-of-principle studies of light nuclei within small model spaces, I have shown that energy spectra computed from the time-evolved excitation amplitudes indeed replicate results obtained within the well-known time-independent formalism; the coupled-cluster energy functional is and remains well-conserved under time-evolution of the excitation and de-excitation amplitudes; and the imaginary-time evolution of the similarity-transformed Hamiltonian is useful in the suppression of excitations and thus the determination of ground-state properties.

I have not done a computation involving the dynamic of interacting nuclei. Based on the quality of the results shown here, I do however speculate that this method will be useful in studying nuclear collisions—i.e., fission and fusion reactions—at an accuracy beyond that of current mean-field descriptions of such phenomena. The requisites for doing so, in addition to the formulation presented in Chapter 2, are equations which govern the time-evolution of the occupied and unoccupied single-particle states. In his article [31], Kvaal presents such equations. The computational feasibility of such an application using a realistic model space is to be determined.

APPENDIX A

EQUATIONS (29)-(31) IN A TIME-DEPENDENT BASIS

If the orbitals are allowed to time-evolve, all terms within the expansion of $e^{-S}\partial_t e^S$ [see Eq. (28)] contribute to the time-evolution of the excitation amplitudes s_o, s_i^a, and s_{ij}^{ab}. In this case Eqs. (29)-(31) become

$$\langle \Phi | \, \overline{H}_S \, | \Phi \rangle = i\hbar \Big[\dot{s}_0 + \sum_k \langle k | \dot{k} \rangle + \sum_{kc} s_k^c \, \langle k | \dot{c} \rangle \Big] \tag{87}$$

$$\begin{aligned} \langle \Phi_i^a | \, \overline{H}_S \, | \Phi \rangle = i\hbar \Big[& \dot{s}_i^a + \langle a | \dot{i} \rangle \\ & + \sum_c s_i^c \, \langle a | \dot{c} \rangle + \sum_k s_k^a \, \langle i | \dot{k} \rangle^* \\ & + \frac{1}{2} \sum_{kc} s_k^a s_i^c \left(\langle c | \dot{k} \rangle^* - \langle k | \dot{c} \rangle \right) \\ & + \sum_{kc} s_{ki}^{ca} \left(\langle k | \dot{c} \rangle + \langle c | \dot{k} \rangle^* \right) \Big] \end{aligned} \tag{88}$$

$$\begin{aligned} \left\langle \Phi_{ij}^{ab} \right| \overline{H}_S \, | \Phi \rangle = i\hbar \Big[& \dot{s}_{ij}^{ab} + \sum_c \left(s_{ij}^{cb} \, \langle a | \dot{c} \rangle - s_{ij}^{ca} \, \langle b | \dot{c} \rangle \right) \\ & + \sum_k \left(s_{kj}^{ab} \, \langle i | \dot{k} \rangle - s_{ki}^{ab} \, \langle j | \dot{k} \rangle \right) \\ & + \frac{1}{2} P(ab) \sum_{kc} s_k^a s_{ij}^{cb} \left(\langle c | \dot{k} \rangle^* - \langle k | \dot{c} \rangle \right) \\ & + \frac{1}{2} P(ij) \sum_{kc} s_i^c s_{kj}^{ab} \left(\langle c | \dot{k} \rangle^* - \langle k | \dot{c} \rangle \right) \Big] \, , \end{aligned} \tag{89}$$

where the permutation operator P is defined as $P(pq) f(p,q) \equiv f(p,q) - f(q,p)$. The derivation of the additional terms here involves a straightforward application of Eq. (12).

APPENDIX B

STRUCTURES OF DIAGRAM FRAGMENTS

In Figs. 24-27, the structures of the diagram fragments for F_N, G_N, S, and Λ are shown, respectively. Note that these diagram fragments correspond to a CCSD implementation using a two-body Hamiltonian. Higher-order truncations of S and Λ require the addition of S_n and Λ_n fragments, where $n > 2$; and the utilization of an n-body Hamiltonian, where $n > 2$, requires the addition of all possible $3, \ldots, n$-body interaction fragments.

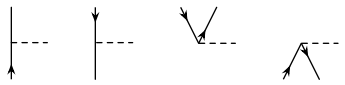

Figure 24. Structures of the elements of F_N. From left to right, they are f^a_b, f^i_j, f^a_i, and f^i_a.

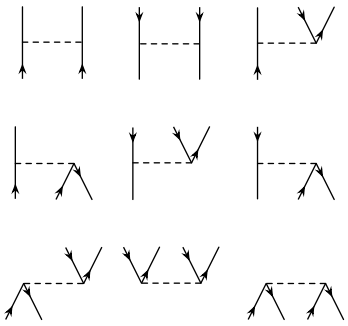

Figure 25. Structures of the elements of G_N. Row by row, from left to right, they are g^{ab}_{cd}, g^{ij}_{kl}, g^{ab}_{ci}, g^{ai}_{bc}, g^{ia}_{jk}, g^{ik}_{ja}, g^{ja}_{bi}, g^{ab}_{ij}, and g^{ij}_{ab}.

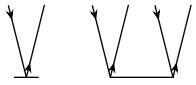

Figure 26. Structures of the excitation amplitudes s_i^a and s_{ij}^{ab}.

Figure 27. Structures of the de-excitation amplitudes λ_a^i and λ_{ab}^{ij}.

APPENDIX C

RULES FOR INTERPRETING DIAGRAMS

T. D. Crawford and H. F. Schaefer [37] and I. Shavitt and R. J. Bartlett [4] provide thorough explanations of the rules for obtaining algebraic expressions from coupled-cluster diagrams. A summary of the rules is given here, and Fig. 28 is referenced throughout.

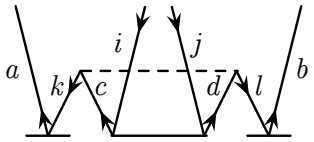

Figure 28. Diagram contributing to the element $\left\langle \Phi_{ij}^{ab} \right| \overline{H}_S \left| \Phi \right\rangle$.

1. Label hole lines, directed downward, with indices $i, j, k, \ldots$ and particle lines, directed upward, with indices $a, b, c, \ldots$. This is already done in Fig. 28.
2. For a one-body interaction vertex, a two-body interaction vertex, an *np-nh* excitation amplitude, or an *nh-np* de-excitation amplitude, associate a factor f_{in}^{out}, $g_{in_1\ in_2}^{out_1\ out_2}$, $s_{i_1 \ldots i_n}^{a_1 \ldots a_n}$, and $\lambda_{a_1 \ldots a_n}^{i_1 \ldots i_n}$, respectively. For the diagram in Fig. 28, the product looks like $g_{cd}^{kl} s_k^a s_{ij}^{cd} s_l^b$.
3. Introduce a summation over all indices associated with internal lines, lines which connect two vertices. In the diagram in Fig. 28, lines k, l, c, and d are internal lines; thus the expression now looks like $\sum_{klcd} g_{cd}^{kl} s_k^a s_{ij}^{cd} s_l^b$. External lines, however, are lines which are connected to only one vertex—i.e., they are not shared between fragments; thus they are not summed over. Rather, their indices identify the element to which the diagram contributes. The diagram in Fig. 28, within which the lines i, j, a, and b are external lines, contributes to the element

$\left\langle \Phi_{ij}^{ab} \right| \overline{H}_S \left| \Phi \right\rangle \equiv \overline{H}_{ij}^{ab}$.

4. Associate a factor of 1/2 for each pair of equivalent lines. Internal lines which connect the same two fragments of a diagram and are either both particle or holes lines are considered equivalent lines. The factor of 1/2 is essential because the summation over the associated indices is unrestricted. In the diagram in Fig. 28, lines c and d are equivalent; thus a factor of 1/2 is needed. The expression now looks like $\frac{1}{2} \sum_{klcd} g_{cd}^{kl} s_k^a s_{ij}^{cd} s_l^b$.
5. Associate a factor of 1/2 for each pair of equivalent S or Λ amplitudes. Amplitudes which have the same number of vertices and are connected in the same way to an interaction fragment are considered equivalent. The factor of 1/2 is essential because the amplitudes can be interchanged to reproduce the diagram; thus the intended contribution is accounted for twice in the unrestricted summation. In the diagram in Fig. 28, the two S_1 vertices, associated with amplitudes s_k^a and s_l^b, are equivalent; thus a factor of 1/2 is needed. The expression now looks like $\frac{1}{4} \sum_{klcd} g_{cd}^{kl} s_k^a s_{ij}^{cd} s_l^b$.
6. Associate an overall sign of -1^{h-l}, where h is the number of hole lines and l is the number of loops, both internal and external. An internal loop is defined as one that can be explicitly traced back to its origin, and an external loop is simply a pair of external lines, one representing a particle and the other a hole and both emanating from either the top or bottom of a diagram. It can be shown that the full contraction of each string of second-quantized operators corresponding to one diagrammatic loop carries a sign of -1^{h-1}; thus it can be deduced that the overall sign of a diagram containing l loops is -1^{h-l}. The diagram in Fig. 28 contains four hole lines (i, j, k, and l) and two external loops ($a_a^\dagger a_i$ and $a_b^\dagger a_j$); thus its algebraic representation has a sign of $-1^2 = +1$.
7. Associate a permutation operator $P(pq)$, where $P(pq)f(p,q) \equiv f(p,q) - f(q,p)$, for each pair of unique external particle or hole lines emanating from different

fragments. This is done to ensure that the expression is antisymmetric with respect to the associated indices. For example, the diagram in Fig. 28 contributes to the element $\overline{H}^{ab}_{ij}$, so we must ensure that $\overline{H}^{ab}_{ij} = -\overline{H}^{ab}_{ji} = -\overline{H}^{ba}_{ij} = \overline{H}^{ba}_{ji}$. To do this, we must explicitly permute the indices a and b since they belong to different fragments, the vertices associated with amplitudes s^a_k and s^b_l. Since the amplitude s^{cd}_{ij} is already antisymmetric with respect to indices i and j, they need not be explicitly permuted. The expression now looks like $\frac{1}{4}P(ab)\sum_{klcd} g^{kl}_{cd} s^a_k s^{cd}_{ij} s^b_l$.

8. A permutation factor $P(pq)$ can be cancelled with a factor of $1/2$ provided that lines p and q are connected to equivalent amplitudes. This is due to the fact that the presence of both factors $1/2$ and $P(pq)$ renders the summation over indices p and q effectively restrictive. In Fig. 28, lines a and b are connected to equivalent S_1 vertices, associated with amplitudes s^a_k and s^b_l; thus $\frac{1}{2}P(ab)$ can be factored from the expression, leaving $\frac{1}{2}\sum_{klcd} g^{kl}_{cd} s^a_k s^{cd}_{ij} s^b_l$ as the final expression for the diagram.

APPENDIX D

ADDITIONAL ELEMENTS OF $\overline{H}_S$

Shown here are the diagrammatic and algebraic expansions of all of the elements of $\overline{H}_S$ needed within a CCSD calculation and not provided elsewhere in the text.

One-Body Elements

In addition to the element $\overline{H}_i^a$, for which the diagrammatic and algebraic expansions are presented in Fig. 4 and Eq. (34), the one-body elements of $\overline{H}_S$ include $\overline{H}_a^i$, $\overline{H}_b^a$, and $\overline{H}_j^i$. The diagrammatic expansions of $\overline{H}_a^i$ and $\overline{H}_b^a$ are shown in Fig. 29. The diagrams contributing to $\overline{H}_j^i$ are formed simply by reversing the direction of all of the arrows in the diagrams contributing to $\overline{H}_b^a$. The algebraic expressions corresponding to these elements are given by

$$\overline{H}_a^i = f_a^i + \sum_{jb} g_{ab}^{ij} s_j^b \tag{90}$$

$$\overline{H}_b^a = f_b^a + \sum_{ic} g_{bc}^{ai} s_i^c - \sum_i \overline{H}_b^i s_i^a - \frac{1}{2} \sum_{ijc} g_{bc}^{ij} s_{ij}^{ac} \tag{91}$$

$$\overline{H}_j^i = f_j^i + \sum_{ka} g_{ja}^{ik} s_k^a + \sum_a \overline{H}_a^i s_j^a + \frac{1}{2} \sum_{kab} g_{ab}^{ik} s_{jk}^{ab} \; . \tag{92}$$

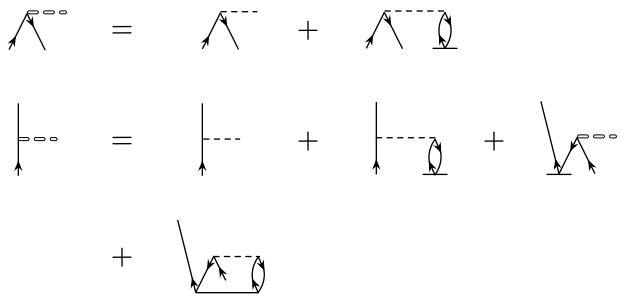

Figure 29. Diagrammatic expansions of $\overline{H}_a^i$ and $\overline{H}_b^a$, respectively.

Two-Body Elements

In addition to the element $\overline{H}_{ij}^{ab}$, presented in Figs. 5 and 6 and Eq. (35), the two-body elements of $\overline{H}_S$ include $\overline{H}_{cd}^{ab}$, $\overline{H}_{kl}^{ij}$, $\overline{H}_{ci}^{ab}$, $\overline{H}_{jk}^{ia}$, $\overline{H}_{bc}^{ai}$, $\overline{H}_{ja}^{ik}$, $\overline{H}_{bi}^{ja}$, and $\overline{H}_{ab}^{ij}$. The diagrammatic expansions of $\overline{H}_{cd}^{ab}$, $\overline{H}_{ci}^{ab}$, $\overline{H}_{bc}^{ai}$, $\overline{H}_{bi}^{ja}$, and $\overline{H}_{ab}^{ij}$ are shown in Fig. 30. Diagrams contributing to $\overline{H}_{kl}^{ij}$, $\overline{H}_{jk}^{ia}$, and $\overline{H}_{ja}^{ik}$ are formed by reversing the direction of all arrows in the expansions of $\overline{H}_{cd}^{ab}$, $\overline{H}_{ci}^{ab}$, and $\overline{H}_{bc}^{ai}$, respectively. The algebraic expressions corresponding to these elements are given by

$$\overline{H}_{ab}^{ij} = g_{ab}^{ij} \tag{93}$$

$$\overline{H}_{bi}^{ja} = g_{bi}^{ja} + \sum_{c} g_{bc}^{ja} s_i^c - \sum_{k} g_{bi}^{jk} s_k^a - \sum_{kc} g_{bc}^{jk} s_i^c s_k^a + \sum_{kc} g_{bc}^{jk} s_{ki}^{ca} \tag{94}$$

$$\overline{H}_{cd}^{ab} = g_{cd}^{ab} - P(ab) \sum_{i} g_{cd}^{ai} s_i^b + \sum_{ij} g_{cd}^{ij} s_i^a s_j^b + \frac{1}{2} \sum_{ij} g_{cd}^{ij} s_{ij}^{ab} \tag{95}$$

$$\overline{H}_{kl}^{ij} = g_{kl}^{ij} + P(kl) \sum_{a} g_{ka}^{ij} s_l^a + \sum_{ab} g_{ab}^{ij} s_k^a s_l^b + \frac{1}{2} \sum_{ab} g_{ab}^{ij} s_{kl}^{ab} \tag{96}$$

$$\begin{aligned} \overline{H}_{ci}^{ab} = {} & g_{ci}^{ab} - P(ab) \sum_{j} g_{ci}^{aj} s_j^b + \sum_{d} g_{cd}^{ab} s_i^d + \sum_{jk} g_{ci}^{jk} s_j^a s_k^b \\ & - P(ab) \sum_{jd} g_{cd}^{aj} s_i^d s_j^b + \sum_{jkd} g_{cd}^{jk} s_j^a s_i^d s_k^b - P(ab) \sum_{jkd} g_{cd}^{jk} s_j^a s_{ki}^{db} \\ & + \sum_{jkd} g_{cd}^{jk} s_j^d s_{ki}^{ab} + \frac{1}{2} \sum_{jkd} g_{cd}^{jk} s_{jk}^{ab} s_i^d - \sum_{j} f_c^j s_{ji}^{ab} \\ & + P(ab) \sum_{jd} g_{cd}^{aj} s_{ji}^{db} + \frac{1}{2} \sum_{jk} g_{ci}^{jk} s_{jk}^{ab} \end{aligned} \tag{97}$$

$$\begin{aligned} \overline{H}_{jk}^{ia} = {} & g_{jk}^{ia} - \sum_{l} g_{jk}^{il} s_l^a + P(jk) \sum_{b} g_{jb}^{ia} s_k^b + \sum_{bc} g_{bc}^{ia} s_j^b s_k^c \\ & - P(jk) \sum_{lb} g_{jb}^{il} s_k^b s_l^a - \sum_{lbc} g_{bc}^{il} s_j^b s_k^c s_l^a + P(jk) \sum_{lbc} g_{bc}^{il} s_j^b s_{lk}^{ca} \\ & - \sum_{lbc} g_{bc}^{il} s_l^b s_{jk}^{ca} - \frac{1}{2} \sum_{lbc} g_{bc}^{il} s_{jk}^{bc} s_l^a + \sum_{b} f_b^i s_{jk}^{ba} \\ & + P(jk) \sum_{lb} g_{jb}^{il} s_{lk}^{ba} + \frac{1}{2} \sum_{bc} g_{bc}^{ia} s_{jk}^{bc} \end{aligned} \tag{98}$$

$$\overline{H}_{bc}^{ai} = g_{bc}^{ai} - \sum_{j} g_{bc}^{ji} s_j^a \tag{99}$$

$$\overline{H}^{ik}_{ja} \;=\; g^{ik}_{ja} + \sum_b g^{ik}_{ba} s^b_j \;. \tag{100}$$

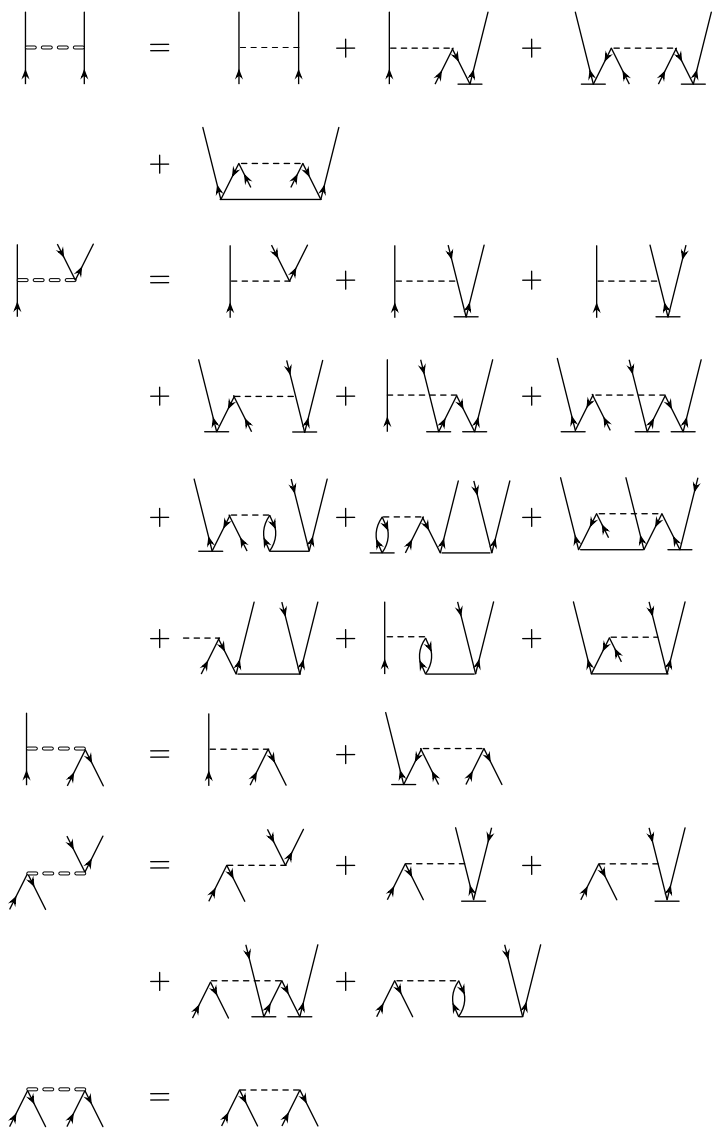

Figure 30. Diagrammatic expansions of $\overline{H}^{ab}_{cd}$, $\overline{H}^{ab}_{ci}$, $\overline{H}^{ai}_{bc}$, $\overline{H}^{ja}_{bi}$, and $\overline{H}^{ij}_{ab}$.

Three-Body Elements

In the CCSD approximation, the only three-body elements of $\overline{H}_S$ needed within

computations are $\overline{H}^{ibc}_{ajk}$, $\overline{H}^{jab}_{cdi}$, and $\overline{H}^{ija}_{kbl}$. The diagrammatic expansions of $\overline{H}^{ibc}_{ajk}$ and $\overline{H}^{jab}_{cdi}$ are shown in Fig. 31. Diagrams contributing to $\overline{H}^{ija}_{kbl}$ are obtained by reversing the direction of all arrows in the expansion of $\overline{H}^{jab}_{cdi}$. The algebraic expressions corresponding to these elements are given by

$$\overline{H}^{ibc}_{ajk} = \sum_d \overline{H}^{ib}_{ad} s^{dc}_{jk} - \sum_l \overline{H}^{il}_{aj} s^{bc}_{lk} \tag{101}$$

$$\overline{H}^{ajb}_{cdi} = -\sum_k g^{jk}_{cd} s^{ab}_{ki} \tag{102}$$

$$\overline{H}^{ija}_{kbl} = \sum_c g^{ij}_{bc} s^{ca}_{kl} \ . \tag{103}$$

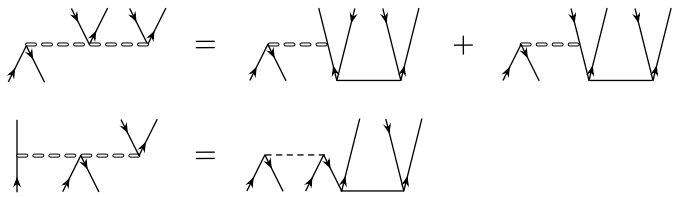

Figure 31. Diagrammatic expansions of $\overline{H}^{ibc}_{ajk}$ and $\overline{H}^{ajb}_{cdi}$.

APPENDIX E

CCSD ONE-BODY AND TWO-BODY DENSITIES

The diagrammatic and algebraic expansions of the normal-ordered one-body and two-body densities are provided in the CCSD approximation.

One-Body Density

The diagrammatic expansions of the normal-ordered one-body densities are given in Fig. 32. Note several things here. First, within the diagrams I have represented vertices as small circles, which serve as placeholders for diagram fragments associated with observables. It is understood that the "real" density vertices oppose those represented by the circles; for this reason the *in* and *out* indices of ρ_{in}^{out} are inverted relative to the circles. Second, the only difference between the one-body density and its normal-ordered form lies in the hole-hole elements; for this reason the N subscript has been suppressed from the other elements. Finally, the diagrams contributing to $(\rho_i^j)_N$ are formed by reversing the direction of all arrows in those contributing to ρ_a^b. The associated algebraic expansions are given by

$$\rho_a^b = \sum_i s_i^b \lambda_a^i + \sum_{ijc} s_{ij}^{cb} \lambda_{ca}^{ij} \tag{104}$$

$$(\rho_i^j)_N = -\sum_a s_i^a \lambda_a^j - \frac{1}{2} \sum_{kab} s_{ki}^{ab} \lambda_{ab}^{kj} \tag{105}$$

$$\rho_a^i = \lambda_a^i \tag{106}$$

$$\rho_i^a = s_i^a - \sum_{jb} s_i^b s_j^a \lambda_b^j + \sum_{jb} s_{ji}^{ba} \lambda_b^j - \frac{1}{2} \sum_{jkbc} s_{jk}^{ba} s_i^c \lambda_{bc}^{jk} - \frac{1}{2} \sum_{jkbc} s_{ji}^{bc} s_k^a \lambda_{bc}^{jk} \ . \tag{107}$$

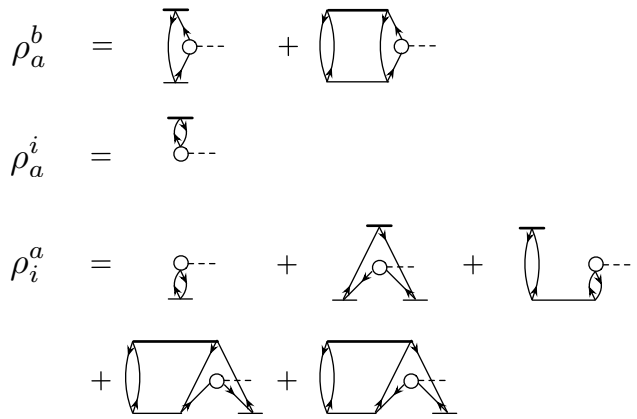

Figure 32. Diagrammatic expansions of normal-ordered one-body densities.

Two-Body Density

The diagrammatic expansions of the normal-ordered two-body densities are divided between Figs. 33 and 34. Note that diagrams for the elements $(\rho_{ij}^{kl})_N$, $(\rho_{ik}^{ja})_N$, and $(\rho_{ia}^{jk})_N$ are formed by reversing the directions of all arrows in those contributing to ρ_{ab}^{cd}, ρ_{ai}^{bc}, and ρ_{ab}^{ci}, respectively. In cases where there is no difference between a given density and its normal-ordered form, the N subscript has been suppressed. The associated algebraic expansions are given by

$$\rho_{ab}^{cd} = \frac{1}{2}\sum_{ij} s_i^c s_j^d \lambda_{ab}^{ij} + \frac{1}{8}\sum_{ij} s_{ij}^{cd} \lambda_{ab}^{ij} \tag{108}$$

$$(\rho_{ij}^{kl})_N = \frac{1}{2}\sum_{ab} s_i^a s_j^b \lambda_{ab}^{kl} + \frac{1}{8}\sum_{ab} s_{ij}^{ab} \lambda_{ab}^{kl} \tag{109}$$

$$\rho_{ab}^{ci} = \frac{1}{2}\sum_{j} s_j^c \lambda_{ab}^{ji} \tag{110}$$

$$(\rho_{ia}^{jk})_N = -\frac{1}{2}\sum_{b} s_i^b \lambda_{ab}^{jk} \tag{111}$$

$$\begin{aligned}\rho_{ai}^{bc} = {} & P(bc)\sum_{j} s_j^b s_i^c \lambda_a^j + \frac{1}{2}\sum_{j} s_{ji}^{bc} \lambda_a^j - \sum_{jkd} s_j^b s_k^c s_i^d \lambda_{ad}^{jk} - \frac{1}{4}\sum_{jkd} s_{jk}^{bc} s_i^d \lambda_{ad}^{jk} \\ & + P(bc)\sum_{jkd} s_j^b s_{ik}^{cd} \lambda_{ad}^{jk} + \frac{1}{2}P(bc)\sum_{jkd} s_{jk}^{db} s_i^c \lambda_{da}^{jk}\end{aligned} \tag{112}$$

$$
\begin{aligned}
(\rho^{ja}_{ik})_N &= -P(ik)\sum_b s^b_i s^a_k \lambda^j_b - \frac{1}{2}\sum_b s^{ba}_{ik}\lambda^j_b + \sum_{lbc} s^b_i s^c_k s^a_l \lambda^{jl}_{bc} \qquad (113)\\
&+ \frac{1}{4}\sum_{lbc} s^{ba}_{il} s^c_k \lambda^{jl}_{bc} - P(ik)\sum_{lbc} s^b_i s^{ac}_{kl}\lambda^{jl}_{bc} - \frac{1}{2}P(ik)\sum_{lbc} s^{bc}_{li} s^a_k \lambda^{lj}_{bc}\\
(\rho^{bi}_{ja})_N &= s^b_j \lambda^i_a - \sum_{kc} s^b_k s^c_j \lambda^{ki}_{ca} + \sum_{kc} s^{bc}_{jk}\lambda^{ik}_{ac} \qquad (114)\\
\rho^{ij}_{ab} &= \lambda^{ij}_{ab} \qquad (115)\\
\rho^{ab}_{ij} &= P(ij|ab)s^a_i s^b_j + s^{ab}_{ij} - P(ij|ab)\sum_{kc} s^a_k s^c_i s^b_j \lambda^k_c - \frac{1}{2}P(ab)\sum_{kc} s^a_k s^{cb}_{ij}\lambda^k_c \qquad (116)\\
&- \frac{1}{2}P(ij)\sum_{kc} s^c_i s^{ab}_{kj}\lambda^k_c + P(ij|ab)\sum_{kc} s^{ca}_{ki} s^b_j \lambda^k_c + \sum_{klcd} s^a_k s^c_i s^b_l s^d_j \lambda^{kl}_{cd}\\
&+ \frac{1}{4}\sum_{klcd} s^c_i s^{ab}_{kl} s^d_j \lambda^{kl}_{cd} + \frac{1}{4}\sum_{klcd} s^a_k s^{cd}_{ij} s^b_l \lambda^{kl}_{cd} - \frac{1}{2}P(ij|ab)\sum_{klcd} s^{ca}_{kl} s^d_i s^b_j \lambda^{kl}_{cd}\\
&- \frac{1}{2}P(ij|ab)\sum_{klcd} s^{cd}_{ki} s^a_l s^b_j \lambda^{kl}_{cd} - P(ij|ab)\sum_{klcd} s^a_k s^c_i s^{bd}_{jl}\lambda^{kl}_{cd}\\
&+ P(ij)\sum_{klcd} s^{ca}_{ki} s^{bd}_{jl}\lambda^{kl}_{cd} + \frac{1}{16}\sum_{klcd} s^{ab}_{kl} s^{cd}_{ij}\lambda^{kl}_{cd} - \frac{1}{4}P(ab)\sum_{klcd} s^{ca}_{kl} s^{db}_{ij}\lambda^{kl}_{cd}\\
&- \frac{1}{4}P(ij)\sum_{klcd} s^{cd}_{ki} s^{ab}_{lj}\lambda^{kl}_{cd}\ .
\end{aligned}
$$

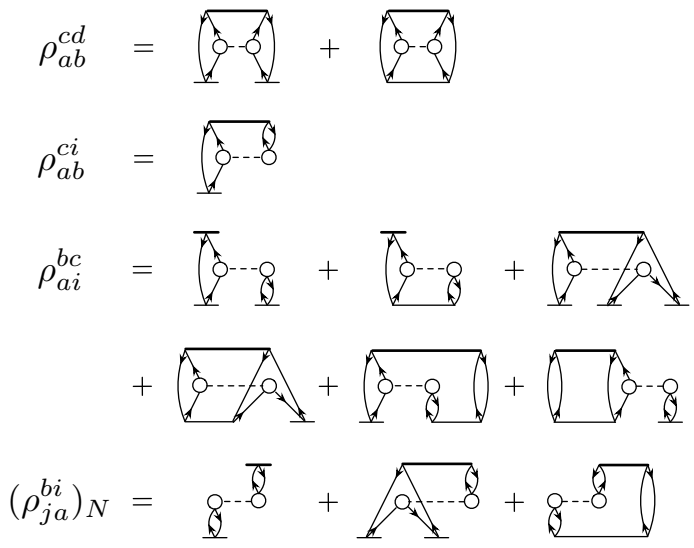

Figure 33. Diagrammatic expansions of normal-ordered two-body densities.

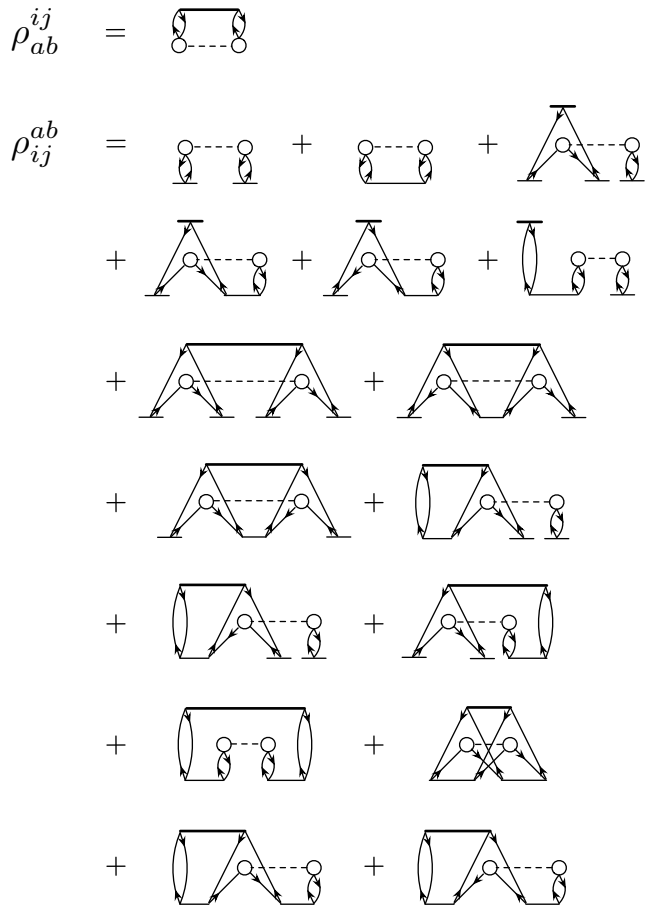

Figure 34. Diagrammatic expansions of normal-ordered two-body densities.

APPENDIX F

EQUATIONS OF MOTION

Given here are the diagrammatic and algebraic expansions of the EOM-CCSD equations for the right and left eigenvalue problems of $\overline{H}$ and the EOM-CCSDT equations when only $S_1 \neq 0$—i.e., $S_n = 0$, $n > 1$—for the right eigenvalue problem of $\overline{H}$.

EOM-CCSD: The Right Eigenvalue Problem of $\overline{H}$

Eqs. (60)-(62) are the working equations for the right eigenvalue problem of $\overline{H}$. The diagrammatic expansions of the left-hand sides of the equations are shown in Figs. 35-37, respectively. Note from the figures that the R vertices are represented with thick lines in order to distinguish them from S vertices. The algebraic expressions associated with the figures are given, respectively, by

$$\omega r_0 = \sum_{ia} \overline{H}_a^i r_i^a + \frac{1}{4} \sum_{ijab} \overline{H}_{ab}^{ij} r_{ij}^{ab} \tag{117}$$

$$\begin{aligned} \omega r_i^a = & \sum_b \overline{H}_b^a r_i^b - \sum_j \overline{H}_i^j r_j^a + \sum_{jb} \overline{H}_{bi}^{ja} r_j^b + \sum_{jb} \overline{H}_b^j r_{ij}^{ab} \\ & + \frac{1}{2} \sum_{jbc} \overline{H}_{bc}^{aj} r_{ij}^{bc} - \frac{1}{2} \sum_{jkb} \overline{H}_{ib}^{jk} r_{jk}^{ab} \end{aligned} \tag{118}$$

$$\begin{aligned} \omega r_{ij}^{ab} = & P(ij) \sum_c \overline{H}_{cj}^{ab} r_i^c - P(ab) \sum_k \overline{H}_{ij}^{kb} r_k^a + \sum_{kc} \overline{H}_{cij}^{kab} r_k^c \\ & + P(ab) \sum_c \overline{H}_c^b r_{ij}^{ac} - P(ij) \sum_k \overline{H}_j^k r_{ik}^{ab} + \frac{1}{2} \sum_{cd} \overline{H}_{cd}^{ab} r_{ij}^{cd} \\ & + \frac{1}{2} \sum_{kl} \overline{H}_{ij}^{kl} r_{kl}^{ab} + P(ab|ij) \sum_{kc} \overline{H}_{cj}^{kb} r_{ik}^{ac} + \frac{1}{2} P(ij) \sum_{kcd} \overline{H}_{cdj}^{akb} r_{ik}^{cd} \\ & - \frac{1}{2} P(ab) \sum_{klc} \overline{H}_{icj}^{klb} r_{kl}^{ac} \ . \end{aligned} \tag{119}$$

Figure 35. Diagrammatic expansion of $\langle\Phi|\,[\overline{H}_S, R]\,|\Phi\rangle$.

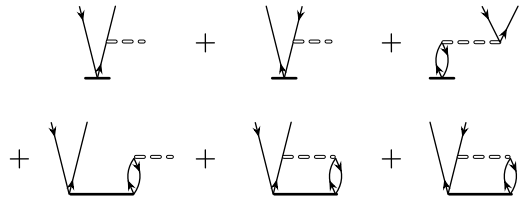

Figure 36. Diagrammatic expansion of $\langle\Phi_i^a|\,[\overline{H}_S, R]\,|\Phi\rangle$.

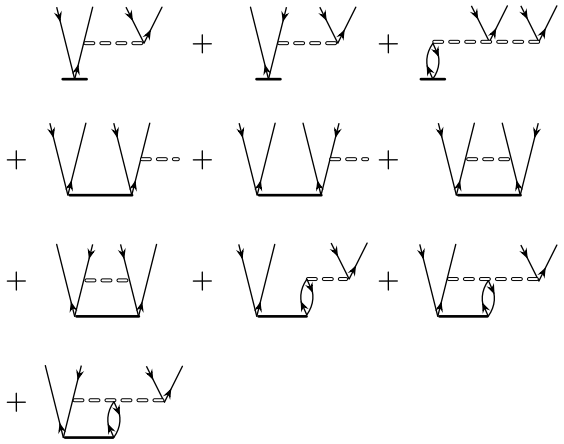

Figure 37. Diagrammatic expansion of $\langle\Phi_{ij}^{ab}|\,[\overline{H}_S, R]\,|\Phi\rangle$.

EOM-CCSD: The Left Eigenvalue Problem of $\overline{H}$

The working equations for the left eigenvalue problem of $\overline{H}$ are Eqs. (65)-(67). The diagrammatic expansion of the left-hand side of Eq. (65) is given in Fig. 38 while those of the left-hand sides of Eqs. (66) and (67) are in fact identical to those associated with the de-excitation operator Λ, given in Figs. 7 and 8, respectively, with the exception that the diagrams which depend on the elements $\overline{H}_i^a$ and $\overline{H}_{ij}^{ab}$ must also

be included. In this case, the only such contribution is to the L_1 diagrams, and it is shown in Fig. 39. The algebraic expressions associated with the diagrams given in the figures are, respectively,

$$\omega l_0 \;=\; \sum_{ia} \overline{H}_i^a l_a^i + \frac{1}{4} \sum_{ijab} \overline{H}_{ij}^{ab} l_{ab}^{ij} \tag{120}$$

and

$$\omega l_a^i \;\leftarrow\; \sum_{jb} \overline{H}_j^b l_{ab}^{ij} \;, \tag{121}$$

where it is understood that the remainder of ωl_a^i is given by all of the terms on the right-hand side of Eq. (42), whereby $\lambda_a^i \rightarrow l_a^i$. Furthermore, ωl_{ab}^{ij} is given by the terms on the right-hand side of Eq. (43), whereby $\lambda_{ab}^{ij} \rightarrow l_{ab}^{ij}$.

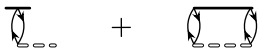

Figure 38. Diagrammatic expansion of $\langle \Phi | \, [L, \overline{H}_S] \, | \Phi \rangle$.

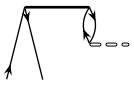

Figure 39. $\overline{H}_{S_1}$ contribution to the diagrammatic expansion of $\langle \Phi | \, [L, \overline{H}_S] \, | \Phi_i^a \rangle$.

EOM-CCSDT: The Right Eigenvalue Problem of $\overline{H}$

The EOM-CCSDT equations for the right eigenvalue problem of $\overline{H}$ comprise Eqs. (60)-(62) in addition to an equation for the $3p$-$3h$ (R_3) amplitude r_{ijk}^{abc}, given by

$$\langle \Phi_{ijk}^{abc} | \, [\overline{H}_S, R] \, | \Phi \rangle \;=\; \omega r_{ijk}^{abc} \;. \tag{122}$$

In my applications of TD-CC thus far, I have solved the EOM-CCSDT equations when only $S_1 \neq 0$. In this approximation, with the addition of r_{ijk}^{abc}, the diagram sums in Figs. 36 and 37 are modified to include the diagrams in Figs. 40 and 41. Eqs. (118) and (119) are thus modified to include

$$\omega r_i^a \leftarrow \frac{1}{4}\sum_{bcjk} \overline{H}_{bc}^{jk} r_{ijk}^{abc} \tag{123}$$

$$\omega r_{ij}^{ab} \leftarrow \sum_{kc} \overline{H}_c^k r_{ijk}^{abc} + \frac{1}{2}P(ab)\sum_{kcd} \overline{H}_{cd}^{bk} r_{ijk}^{acd} - \frac{1}{2}P(ij)\sum_{klc} \overline{H}_{jc}^{kl} r_{ikl}^{abc} \ . \tag{124}$$

Note that r_0 is not modified in this approximation since, when only $S_1 \neq 0$, $\overline{H}$ has no element $\overline{H}_{abc}^{ijk}$ to fully-connect with r_{ijk}^{abc}. The diagrammatic expansion of Eq. (122) is, in this approximation, shown in Fig. 42; the corresponding algebraic expansion is given by

$$\begin{aligned}
\omega r_{ijk}^{abc} &= P(i/jk|a/bc)\overline{H}_{jk}^{bc} r_i^a + P(k/ij|c/ab)\overline{H}_k^c r_{ij}^{ab} \\
&\quad + P(a/bc|k/ij)\sum_d \overline{H}_{dk}^{bc} r_{ij}^{ad} - P(i/jk|c/ab)\sum_l \overline{H}_{jk}^{lc} r_{il}^{ab} \\
&\quad + P(c/ab)\sum_d \overline{H}_d^c r_{ijk}^{abd} - P(k/ij)\sum_l \overline{H}_k^l r_{ijl}^{abc} \\
&\quad + P(c/ab|k/ij)\sum_{ld} \overline{H}_{dk}^{lc} r_{ijl}^{abd} + \frac{1}{2}P(a/bc)\sum_{de} \overline{H}_{de}^{bc} r_{ijk}^{ade} \\
&\quad + \frac{1}{2}P(i/jk)\sum_{lm} \overline{H}_{jk}^{lm} r_{ilm}^{abc} \ .
\end{aligned} \tag{125}$$

Note that the tedious permutation $P(i/jk|a/bc)Z_{ijk}^{abc} = Z_{ijk}^{abc} - Z_{jik}^{abc} - Z_{kji}^{abc} - Z_{ijk}^{bac} - Z_{ijk}^{cba} + Z_{jik}^{bac} + Z_{jik}^{cba} + Z_{kji}^{bac} + Z_{kji}^{bac}$.

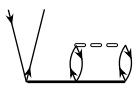

Figure 40. R_3 contribution to the diagrammatic expansion of $\langle \Phi_i^a | \left[\overline{H}_S, R \right] | \Phi \rangle$ when only $S_1 \neq 0$.

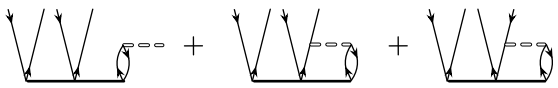

Figure 41. R_3 contribution to the diagrammatic expansion of $\langle \Phi_{ij}^{ab} | \left[\overline{H}_S, R \right] | \Phi \rangle$ when only $S_1 \neq 0$.

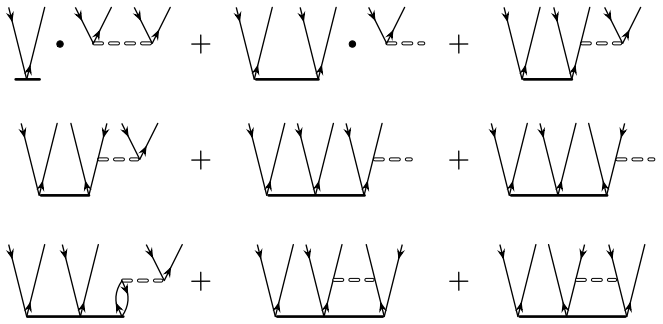

Figure 42. Diagrammatic expansion of $\langle \Phi_{ijk}^{abc} | \left[\overline{H}_S, R \right] | \Phi \rangle$ when only $S_1 \neq 0$.

REFERENCES

[1] B. W. Carroll and D. A. Ostlie, *An Introduction to Modern Astrophysics*, 2nd ed. (Addison-Wesley, 2007).

[2] *Chart of Nuclides* (2012), URL: http://www.nndc.bnl.gov/chart.

[3] *Nuclear Landscape* (2012), URL: http://www.unedf.org.

[4] I. Shavitt and R. J. Bartlett, *Many-Body Methods in Chemistry and Physics: MBPT and Coupled-Cluster Theory* (Cambridge, 2009).

[5] W. Kohn, "Nobel lecture: electronic structure of matter--wave functions and density functionals," Rev. Mod. Phys. **71**, 1253 (1999).

[6] J. Dobaczewski, "Current developments in nuclear density functional methods," J. Phys. Conf. Ser. **312**, 092002 (2011).

[7] A. De Shalit and H. Feshbach, *Theoretical Nuclear Physics: Nuclear Structure* (Wiley, 1974).

[8] R. Machleidt, "Nuclear forces from chiral effective field theory," arXiv: 0704.0807 (2008).

[9] P. Ring and P. Schuck, *The Nuclear Many-Body Problem* (Springer, 1980).

[10] P. Navrátil, J. P. Vary, and B. R. Barrett, "Properties of ^{12}C in the ab initio nuclear shell model," Phys. Rev. Lett. **84**, 5728 (2000).

[11] S. C. Pieper, "Quantum monte carlo calculations of light nuclei," Nuc. Phys. A **751**, 516 (2005).

[12] D. J. Dean and M. Hjorth-Jensen, "Toward coupled-cluster implementations in nuclear structure," AIP Conf. Proc. **656**, 197 (2002).

[13] D. J. Dean, G. Hagen, M. Hjorth-Jensen, and T. Papenbrock, "Computational aspects of nuclear coupled-cluster theory," Comp. Sci. Disc. **1**, 15008 (2008).

[14] F. Coester, "Bound states of a many-particle system," Nuc. Phys. **7**, 421 (1958).

[15] F. Coester and H. Kümmel, "Short-range correlations in nuclear wave functions," Nuc. Phys. **17**, 477 (1960).

[16] G. Hagen, M. Hjorth-Jensen, G. R. Jansen, R. Machleidt, and T. Papenbrock, "Evolution of shell structure in neutron-rich calcium isotopes," arXiv:1204.3612 (2012).

[17] S. A. Kucharski and R. J. Bartlett, "Fifth-order many-body perturbation theory and its relationship to various coupled-cluster approaches," Adv. Quan. Chem. **18**, 281 (1986).

[18] P. Hoodbhoy and J. W. Negele, "Time-dependent coupled-cluster approximation to nuclear dynamics II: general formulation," Phys. Rev. C **19**, 1971 (1979).

[19] P. Hoodbhoy and J. W. Negele, "Time-dependent coupled-cluster approximation to nuclear dynamics I: application to a solvable model," Phys. Rev. C **18**, 2380 (1978).

[20] H. J. Lipkin, N. Meshkov, and A. J. Glick, "Validity of many-body approximation methods for a solvable model I: exact solutions and perturbation theory," Nuc. Phys. **62**, 188 (1965).

[21] E. Dalgaard and H. J. Monkhorst, "Some aspects of the time-dependent coupled-cluster approach to dynamic response functions," Phys. Rev. A **28**, 1217 (1983).

[22] H. Sekino and R. J. Bartlett, "A linear response coupled-cluster theory for excitation energy," Int. J. Quan. Chem. **18**, 255 (1984).

[23] K. L. Sebastian, "Correlation effects in ion neutralization scattering with the use of a time-dependent coupled-cluster approach," Phys. Rev. B **31**, 6976 (1985).

[24] M. Takahashi and J. Paldus, "Time-dependent coupled-cluster approach: excitation energy calculation using an orthogonally spin-adapted formalism," J. Chem. Phys. **85**, 1486 (1986).

[25] H. J. Monkhorst, "Chemical physics without the Born-Oppenheimer approximation: the molecular coupled-cluster method," Phys. Rev. A **36**, 1544 (1987).

[26] H. Koch and J. Jørgensen, "Coupled-cluster response functions," J. Chem. Phys. **93**, 3333 (1990).

[27] G. S. Latha and M. D. Prasad, "Time-dependent coupled-cluster approach to multimode vibronic dynamics," J. Chem. Phys. **105**, 2972 (1996).

[28] M. D. Prasad, "Time-dependent coupled-cluster approach to resonance Raman excitation profiles from general anharmonic surfaces," Int. J. Mol. Sci. **3**, 447 (2002).

[29] C. Huber and T. Klamroth, "Explicitly time-dependent coupled-cluster singles-doubles calculations of laser-driven many-electron dynamics," J. Chem. Phys. **134**, 054113 (2011).

[30] J. Arponen, "Variational principles and linked-cluster exp s expansions for static and dynamic many-body problems," Ann. Phys. **151**, 311 (1983).

[31] S. Kvaal, "Ab-inito quantum dynamics using coupled-cluster," J. Chem. Phys. **136**, 194109 (2012).

[32] P. A. M. Dirac, "Note on exchange phenomena in the Thomas atom," Proc. Cam. Phil. Soc. **26**, 376 (1930).

[33] D. M. Brink, M. J. Giannoni, and M. Vénéroni, "Derivation of an adiabatic time-dependent Hartree-Fock formalism from a variational principle," Nuc. Phys. A **258**, 237 (1976).

[34] A. S. Umar and V. E. Oberacker, "^{64}Ni + ^{132}Sn fusion within the density-constrained time-dependent Hartree-Fock formalism," Phys. Rev. C **76**, 014614 (2007).

[35] H.-D. Meyer, F. Gatti, and G. A. Worth, *Multidimensional Quantum Dynamics: MCTDH Theory and Applications* (Wiley, 2009).

[36] D. A. Pigg, G. Hagen, H. Nam, and T. Papenbrock, "Time-dependent coupled-cluster method for atomic nuclei," Phys. Rev. C **86**, 014308 (2012).

[37] T. Crawford and H. Schaefer, "An introduction to coupled-cluster theory for computational chemists," Rev. Comp. Chem. **14**, 33 (2000).

[38] J. Stanton and R. J. Bartlett, "The equation of motion coupled-cluster method: a systematic biorthogonal approach to molecular excitation energies, transition probabilities, and excited-state properties," J. Chem. Phys. **98**, 7029 (1993).

[39] C. Coulson, "Brillouin's theorem and the Hellmann-Feynman theorem for Hartree-Fock wave functions," Mol. Phys. **20**, 687 (1970).

[40] K. Kowalski, D. J. Dean, M. Hjorth-Jensen, T. Papenbrock, and P. Piecuch, "Coupled-cluster calculations of ground and excited states of nuclei," Phys. Rev. Lett. **92**, 132501 (2004).

[41] G. Hagen, D. J. Dean, M. Hjorth-Jensen, T. Papenbrock, and A. Schwenk, "Benchmark calculations for ^{3}H, ^{4}He, ^{16}O, and ^{40}Ca with ab initio coupled-cluster theory," Phys. Rev. C **76**, 44305 (2007).

[42] E. Xu, J. Shen, Z. Kou, and S. Li, "Coupled-cluster with singles, doubles, and partial higher-order excitations based on the corresponding orbitals: the formulation and test applications for bond breaking processes," J. Chem. Phys. **132**, 134110 (2010).

[43] R. J. Bartlett, C. E. Dykstra, and J. Paldus, *Advanced Theories and Computational Approaches to the Electronic Structure of Molecules* (Springer, 1984).

[44] J. E. Campbell, "On the law of combination of operators bearing on the theory of continuous transformation groups," Proc. Lon. Math. Soc. **28**, 381 (1897).

[45] H. F. Baker, "Alternants and continuous groups," Proc. Lon. Math. Soc., Ser. 2 **3**, 24 (1905).

[46] F. Hausdorff, "Die symbolische exponentialformel in der gruppentheorie," Ber. Verhandl. Sächs. Akad. Wiss. Leipzig, Math.-Naturw. Kl. **58**, 19 (1906).

[47] A. L. Fetter and J. D. Walecka, *Quantum Theory of Many-Particle Systems* (McGraw-Hill, 1971).

[48] G. Hagen, T. Papenbrock, D. J. Dean, A. Schwenk, A. Nogga, M. Wloch, and P. Piecuch, "Coupled-cluster theory for three-body Hamiltonians," Phys. Rev. C **76**, 34302 (2007).

[49] P. Piecuch and R. J. Bartlett, "EOMXCC: a new coupled-cluster method for electronic excited states," Adv. Quan. Chem. **34**, 295 (1999).

[50] P. M. Morse and H. Feshbach, *Methods of Theoretical Physics* (McGraw-Hill, 1953).

[51] J. Gour, P. Piecuch, M. Hjorth-Jensen, M. Wloch, and D. J. Dean, "Coupled-cluster calculations for valence systems around ^{16}O," Phys. Rev. C **74**, 24310 (2006).

[52] G. Hagen, T. Papenbrock, and M. Hjorth-Jensen, "Ab-initio computation of the ^{17}F halo state and resonances in A=17 nuclei," Phys. Rev. Lett. **104**, 182501 (2010).

[53] W. E. Arnoldi, "The principle of minimized iterations in the solution of the matrix eigenvalue problem," Quart. App. Math **9**, 17 (1951).

[54] S. K. Bogner, R. J. Furnstahl, and A. Schwenk, "From low-momentum interactions to nuclear structure," Prog. Part. Nucl. Phys. **65**, 94 (2010).

[55] D. R. Entem and R. Machleidt, "Accurate charge-dependent nucleon-nucleon potential at fourth order of chiral perturbation theory," Phys. Rev. C **68**, 041001 (2003).

[56] D. G. Zill and M. R. Cullen, *Differential Equations with Boundary-Value Problems* (Brooks/Cole, 2001).

[57] W. H. Press, S. A. Teukolsky, W. T. Vetterline, and B. P. Flannery, *Numerical Recipes in Fortran 90: The Art of Parallel Scientific Computing* (Cambridge, 1986).

[58] P. Pulay, "Convergence acceleration of iterative sequences: the case of SCF iteration," Chem. Phys. Lett. **73**, 393 (1980).

[59] A. Ruhe, "The two-sided Arnoldi algorithm for nonsymmetric eigenvalue problems," in *Matrix Pencils*, Lecture Notes in Mathematics, Eds. B. Kågström and A. Ruhe **973**, 104 (Springer, 1983).

[60] P. Bonche, S. Koonin, and J. W. Negele, "One-dimensional nuclear dynamics in the time-dependent Hartree-Fock approximation," Phys. Rev. C **13**, 1226 (1976).

[61] K. Hagino and G. F. Bertsch, "RPA approach to rotational symmetry restoration in a three-level Lipkin model," Phys. Rev. C **61**, 024307 (2000).

[62] P. A. M. Dirac, *The Principles of Quantum Mechanics*, 4th ed. (Oxford, 1958).

[63] H. J. Monkhorst, " Calculation of properties with the coupled-cluster method," Int. Jour. Quan. Chem. **11**, 421 (1977).

[64] G. Hagen, T. Papenbrock, and D. J. Dean, "Solution of the center-of-mass problem in nuclear structure calculations," Phys. Rev. Lett. **103**, 062503 (2009).

[65] S. D. Glazek and K. G. Wilson, "Renormalization of Hamiltonians," Phys. Rev. D **48**, 5863 (1993).

[66] F. Wegner, "Flow equations for Hamiltonians," Ann. Phys. **506**, 77 (1994).

[67] S. K. Bogner, R. J. Furnstahl, and R. J. Perry, "Similarity renormalization group for nucleon-nucleon interactions," Phys. Rev. C **75**, 061001 (2007).

[68] W. Li, E. R. Anderson, and R. J. Furnstahl, "Similarity renormalization group with novel generators," Phys. Rev. C **84**, 054002 (2011).

[69] K. Tsukiyama, S. K. Bogner, and A. Schwenk, "In-medium similarity renormalization group for nuclei," Phys. Rev. Lett. **106**, 222502 (2011).